Stress transfer through interphase in curved-fiber pull-out test of three-phase composites

P.R. Budarapu[a,d], S. Kumar[a,*], X. Xxxx[b], M. Paggi[c]

[a] *Department of Mechanical and Materials Engineering, Masdar Institute of Science and Technology, Khalifa University of Science and Technology, Abu Dhabi, UAE*
[b] *Department of ...*
[c] *Multi-scale Analysis of Materials Research Unit, IMT School for Advanced Studies Lucca, Piazza San Francesco 19, 55100 Lucca, Italy.*
[d] *School of Mechanical Sciences, Indian Institute of Technology, Bhubaneswar 752050, India*

Abstract

The chemical and physical interactions between the fiber and matrix during the processing of composites results in the formation of a thin nano scale layer around the fiber, known as interphase, whose properties are different from the fiber and matrix. The properties of the interlayer significantly influence the mechanics of load transfer and hence the macroscopic behaviour of composites. Herein, we present a theoretical frame to study the micro-mechanics of stress transfer in a curved fiber pull-out test and to analyse the stress field in the three-phase composite system based on the shear-lag theory. Apart from the assumptions in the shear-lag theory, the radial stresses are neglected here. Explicit expressions are derived for the normal and shear stresses in the fiber, interphase and matrix, as well as the interfacial stresses between the fiber and interphase and the interphase and matrix. The developed methodology has been applied to analyse the stress field in the three-phase composite system, in a nano curved fiber pull-out test. Results from the analytical model are validated with those obtained from a finite element analysis. Furthermore, influence of graded interphase modulus, according to linear and power laws, on the pull-out performance is also investigated. Graded interphases are observed to influence the reduce the interfacial shear stresses by up to 40% as compared to the ungraded interphases. Therefore, the present study can serve as framework to investigate the pull-out characteristics of a curved fiber in nano composites.

Keywords: Polymer nanocomposites; Stress transfer; Curved fiber pull-out performance; Fiber reinforced three-phase composites.

1. Introduction

Load transfer from the matrix to the intact fibers in fiber-reinforced composites occurs primarily by shear. During service, the initial defects in the matrix develop into small cracks. The bond between fiber and matrix fails when the shear stress between the matrix and fiber reaches a threshold. The failure happens through the initiation of a crack at the interface, which further propagates from the matrix crack surface along the fiber, leading to debonding. The debonding is controlled by the fiber debond stress and the rate of increase of stress along the length of debonded fiber due to friction. Some load transfer between fiber and matrix is still possible by the interfacial or frictional forces due to matrix shrinkage onto the fiber during manufacture [1]. This frictional forces produces a non-uniform stress along the debonded fibre. Because of the variable strength of the fiber along the length, the fiber breaks at some distance from the matrix crack-plane where the stress is highest. After fracture, the composite typically shows a matrix crack-plane with fibers protruding from the matrix, known as pull-out. In an infinite matrix with large number of fibers, every fiber is surrounded by similar environment. Therefore, a single fiber pull-out test can give useful information about the micro-mechanics of stress transfer in fiber reinforced composites.

The influence of interface/interphase on the load bearing capacity of the composites can be characterized based on, experimental techniques, such as: fiber pull/push-out tests [2, 3, 4], drag-out test [5], energy dissipation mechanisms [6], microbond or fragmentation tests [7, 8, 9, 10] and numerical simulations like: molecular dynamics studies [11, 12], finite element analysis [13, 14, 15]. Experimental investigations [6] on mechanisms of energy dissipation in polymer nanocomposites indicate that at sufficiently low strains, energy dissipation in composites with high CNT alignment is not a function of applied strain, as no interfacial slip occurs between the

*Corresponding author
Email addresses: pattabhi@iitbbs.ac.in (P.R. Budarapu), kshanmugam@masdar.ac.ae (S. Kumar)

CNTs and polymer. However, at higher strains, interfacial slip also contributes to energy dissipation apart from the significant contribution of friction between CNTs within agglomerates to energy dissipation, due to matrix plasticity and tearing caused by misorientation of CNTs with the loading direction. Advanced techniques such as transmission electron microscopy (TEM) helps in investigating the detailed morphology of intact interphase and chemical compositions between carbon fiber and polymer composite [16]. Moreover, changes in chemical bonding states of different phase regions, gradient of oxygen to carbon ratio and hence the interfacial strength can also be estimated based on the electron energy loss spectroscopy (EELS).

However, experimental characterization of stress transfer through the interphase is an expensive and time consuming process. Therefore, analytical models to analyze the stress transfer through the interphase were developed by considering the homogeneous interphase [17, 18, 19, 7] and gradually extended to inhomogeneous nature of interphase considering a stair-case variation of material properties across the thickness of the interphase layer [20, 21, 22]. However, developing analytical solutions to understand the stress transfer across the interfaces is hopelessly complicated, even for simple geometries. Therefore, various simplified theories have been developed by adopting several assumptions based on the popular shear-lag effect introduced by Cox [23]. One main assumption in the shear-lag analysis is the state of plain-strain, which helps in relating the radial and shear stresses in the equilibrium equations. Nairn examined the suitability of shear-lag approach for stress transfer in unidirectional composites [24], multilayered composites [25] and imperfect interfaces [26], by adopting three more assumptions [24].

The assumptions listed in [24] are the minimum required number of assumptions, but not unique. For example, Hsueh [27, 28] published a series of articles based on plain-strain theory neglecting the radial dependence of axial stresses, which is only justified for sufficiently long fibers. A shear-lag model considering a cohesive fibre-matrix interface has been developed in [29], using a bilinear cohesive damage evolution law to describe the fibre-matrix interface behaviour. A rate-dependent interfacial bond strength has been estimated in [30] for a quasi-static single-fiber pull-out problem. An analytic framework for the analysis of interphasial and interfacial stresses as well as displacements in a 3D axisymmetric system considering isotropic matrix and transversely isotropic fiber and interphase was developed in [31]. In addition, popular analytical models to characterize the interphase stress transfer mechanics include: variational [32, 18] and energy based [33] approaches, effective interphase model (EIM) and uniform replacement model (URM) [34] to study the effect of inhomogeneous interphase with varying elastic properties in the radial direction on the effective elastic moduli of composites reinforced by fibres/spheres, fiber pull-out problem considering homogeneous interphase [35, 36] and inhomogeneous/graded interphase [37, 38, 39, 31], to name a few. An overview of various modeling techniques and computer implementation aspects of carbon nanotube-polymer composites is reported in [40, 41].

Biological materials such as wood and bone, possess many helicoid microstructures at microscale, which can serve as reinforcing elements to transfer stress between crack surfaces and improve the fracture toughness. The pull-out behavior of a helical fiber from an elastic matrix has been analyzed using the finite element method (FEM) in [42]. The authors reported that the presence of helical fibers can provide high pull-out force and large interface areas, resulting in high energy dissipation and hence the high toughness of biological materials. Inclined fiber pull-out process in a fiber, matrix and the interface system has been analyzed based on a numerical model [43], using the cohesive elements to represent bond-slip behavior, for arbitrary fiber orientations. Chen *et al.*, [44, 45] developed the analytical models to estimate the stress-transfer in curved fiber pull-out problem in a two phase (fiber and matrix) system by ignoring: (i) the displacements in the radial direction and (ii) the presence of fiber while estimating the axial strains in the matrix.

In the present work, we present a theoretical framework to study the curved fiber pull-out behaviour in a fiber, interphase and matrix (FIM) system, called 'three phase' system. The study presents: (i) an analytical model to study the influence of interphase on the stress transfer across the interfaces between curved fiber-interphase and interphase-matrix, as compared to a fiber and matrix system and (ii) an analytical model to estimate the influence of grading the elastic modulus of the interphase along the radial direction on the stress transfer.

The article is structured as follows: the curved fiber pull-out problem is introduced in Section 1. Modeling aspects and the estimation of the axial and shear stresses in the fiber, interphase and matrix are explained in Section 2. Details of the analytical model considering the graded interphases are discussed in Section 2.3. The results are discussed in Section 4. Major predictions of the model are summarised in Section 5.

2. Stress field in a three-phase composite with a curved-fiber

In this section, modeling aspects of the curved fiber pull-out problem in a three phase system are discussed. Closed form expressions are derived to estimate the normal stresses along the fiber direction in fiber, interphase and matrix and shear stresses in the interphase and matrix. The analysis is further extended to a straight fiber pull-out problem in a three phase system.

Consider a single curved fiber embedded in a compliant matrix having an interphase between them, as shown in Fig.1(a). Let E^f and ν^f represent the modulus of elasticity and Poisson's ratio of the fiber. The modulus of

elasticity and the Poisson's ratio of the interphase are denoted by E^i and ν^i, respectively. Whereas, the elastic modulus and the Poisson's ratio of the matrix are indicated by E^m and ν^m, respectively. The radii of the fiber, interphase and matrix are denoted by r_1, r_2 and r_3, respectively. The fiber is pulled by a force P_f at the end $s = L$, as shown in Fig.1(a). A curvilinear coordinate system in s and r is considered, in which the tangential stresses in the interphase and matrix along with the interfacial shear stresses between the fiber-interphase and the interphase-matrix are indicated by τ^i_{rs}, τ^m_{rs}, τ_{i1} and τ_{i2}, respectively (see Fig.1(b)). τ_{rs} is the shear stress at radial location r, along the s direction. Equilibrium of stresses when interfaces are intact on a differential fiber element segment ds with included angle $d\theta$ is shown in Fig. 1(c). All the geometric parameters are normalized by the fiber radius $r^f = r_1$, the stresses and elastic modulii are normalized by the Young's modulus of the fiber E^f and hence the forces are normalized by $\pi(r^f)^2E^f$. The normalized quantities are indicated by '*' in the superscript, for e.g., r^*_1 indicates the normalized fiber radius which is equal to $r_1/r_1 = 1$ and $\tau^{m*}_{rs} = \tau^m_{rs}/E^f$. The following assumptions are considered in the analytical formulation: (i) The axial stress distribution is uniform across the fiber cross-section and across the interphase thickness. (ii) The bonds between fiber-interphase and interphase-matrix are perfect. (iii) Fiber carries only the tensile stress. The interphase carries both tensile stresses from the fiber and the shear stresses from the matrix. Therefore, shear transfer is limited only between matrix and interphase

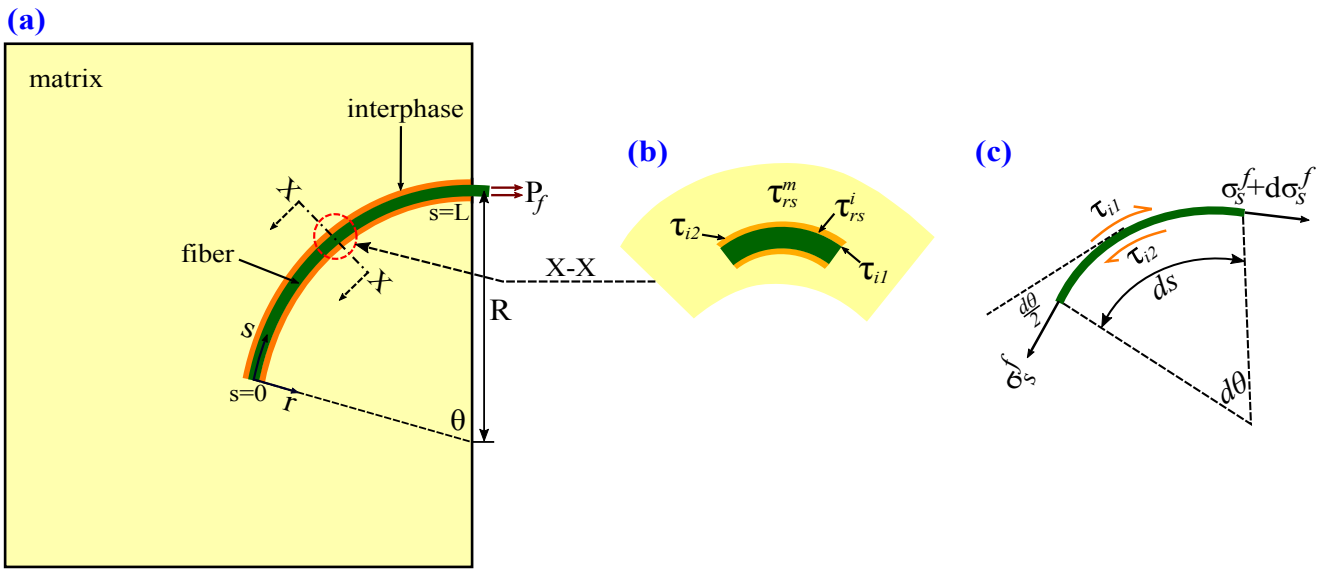

Figure 1: (a) Schematic of a curved fiber pullout having constant radius of curvature R. The curved fiber is embedded in a compliant matrix having an interphase between them. The fiber is pulled by a force P_f at the end $s = L$. Radii of fiber, interphases and matrix are r_1, r_2 and r_3, respectively, in curvilinear coordinate system s and r. (b) Tangential stresses of a matrix segment at section X-X. Shear stresses in the interphase and matrix along with the interfacial shear stresses between fiber-interphase and interphase-matrix are indicated by τ^i_{rs}, τ^m_{rs}, τ_{i1} and τ_{i2}, respectively. (c) Equilibrium of forces in the bonded stage on a differential fiber element segment ds, with included angle $d\theta$.

2.1. Interfacial shear stresses

Let τ^*_{rs} be the normalized shear stress at r along the s direction. The interfacial shear stresses can be estimated satisfying the equilibrium of forces along the fiber direction. According to the shear-lag theory [24], the interfacial shear stresses are given by:

$$\tau^*_i = \tau^*_{rs} r^*, \tag{1}$$

where r^* varies as:

$$r^*_1 \leq r^* \leq r^*_2, \quad \text{in the interphase.} \tag{2}$$

The shear strain (γ_{rs}) can be written as:

$$\gamma_{rs} = \frac{\tau^*_{rs}}{G^*} = \frac{\tau^*_i}{G^* r^*}, \tag{3}$$

where G^* is the normalized shear modulus. The strain-displacement relations in curvilinear co-ordinates can be expressed as [46, 44]:

$$\gamma^{\varrho}_{rs} = \frac{R^*}{R^* - r^{\varrho *}} \frac{\partial u^{\varrho *}_r}{\partial s^*} + \frac{\partial u^{\varrho *}_s}{\partial r^{\varrho *}} + \frac{u^{\varrho *}_s}{R^* - r^{\varrho *}}, \tag{4}$$

where ϱ indicates the member in the three-phase system (fiber (f), interphase (i) and matrix (m)); R is the radius of curvature of the fiber and u^*_r and u^*_s denote the normalized displacement along the r and s directions,

respectively. The variation of the radial displacement along the axial direction is negligible, therefore:

$$\frac{\partial u_r^{\varrho *}}{\partial s^*} \approx 0. \tag{5}$$

Substituting Eqs. (4) and (5) into Eq. (3) yields:

$$\frac{\partial u_s^{i*}}{\partial r^*} + \frac{u_s^{i*}}{R^* - r^*} = \frac{\tau_{i1}^*}{G^{i*} r^*}, \quad \text{for interphase,} \;\; r_1^* \leq r^* \leq r_2^* \tag{6a}$$

$$\frac{\partial u_s^{m*}}{\partial r^*} + \frac{u_s^{m*}}{R^* - r^*} = \frac{\tau_{i2}^*}{G^{m*} r^*}, \quad \text{for matrix,} \;\; r_2^* \leq r^* \leq r_3^*. \tag{6b}$$

where τ_{i1}^*, τ_{i2}^* are the interfacial stresses between the fiber-interphase and interphase-matrix, respectively. Equations (6) are treated as ordinary differential equations. The solutions of Eq. (6) are given by [44]:

$$u_s^{i*}(r^*) = (R^* - r^*)\left[g_i(s) - \frac{\tau_{i1}^*}{G^{i*} R^*} \ln\left(\frac{r^* - R^*}{r^*}\right)\right], \tag{7a}$$

$$u_s^{m*}(r^*) = (R^* - r^*)\left[g_m(s) - \frac{\tau_{i2}^*}{G^{m*} R^*} \ln\left(\frac{r^* - R^*}{r^*}\right)\right], \tag{7b}$$

where $g_i(s)$ and $g_m(s)$ are the arbitrary functions which are estimated based on the boundary conditions. Considering the interface between the fiber and interphase, i.e., $r^* = r_1/r_1 = 1$, $u_s^{i*}(r_1^*) = u_s^{i*}(1)$ and interface between interphase and matrix $r^* = r_2/r_1 = r_2^*$, $u_s^{i*}(r^*) = u_s^{i*}(r_2^*)$; the interfacial shear stresses (τ_{i1}^*, τ_{i2}^*) can be obtained as:

$$\tau_{i1}^* = A_1\left[\frac{u_s^{i*}(r^*)}{(R^* - r^*)} - \frac{u_s^{i*}(1)}{(R^* - 1)}\right], \tag{8a}$$

$$\tau_{i2}^* = A_2\left[\frac{u_s^{m*}(r^*)}{(R^* - r^*)} - \frac{u_s^{m*}(r_2^*)}{(R^* - r_2^*)}\right]. \tag{8b}$$

where A_1 and A_2 are given by:

$$A_1 = \frac{G^{i*} R^*}{\ln\left(\frac{r^*(1-R^*)}{(r^*-R^*)}\right)}, \qquad A_2 = \frac{G^{m*} R^*}{\ln\left(\frac{r^*(r_2^*-R^*)}{r_2^*(r^*-R^*)}\right)}. \tag{9}$$

2.2. Stresses in the fiber

Consider a segment of length ds consisting of fiber, interphase and matrix as shown in Figs. 1(b) and (c). Figure 1(c) shows the force equilibrium of the fiber segment of length ds with subtended angle $d\theta$. The pulling force P_f generates the normal stresses in the fiber, interphase and matrix, as well as the shear stresses in the interphase and matrix. The normal stresses in the fiber are balanced by the interfacial stresses between the fiber-interphase and interphase-matrix. Therefore, equilibrium of forces in the segment leads to:

$$(\sigma_s^{f*} + d\sigma_s^{f*})\pi {r_1^*}^2 \cos\left(\frac{d\theta}{2}\right) - \sigma_s^{f*}\pi {r_1^*}^2 \cos\left(\frac{d\theta}{2}\right) + \tau_{i1}^* 2\pi r_1^* ds^* + \tau_{i2}^* 2\pi r_2^* ds^* = 0. \tag{10}$$

Considering small arc length of the fiber segment, as $d\theta \to 0$, Eq. (10) reduces to:

$$\frac{d\sigma_s^{f*}}{ds^*} = -2[\tau_{i1}^* + \tau_{i2}^* r_2^*]. \tag{11}$$

Substituting τ_{i1}^* and τ_{i2}^* from Eqs. (8) into Eq. (11) yields:

$$\frac{d\sigma_s^{f*}}{ds^*} = -2\mathrm{A}_1\left(\frac{u_s^{i*}(r^*)}{(R^* - r^*)} - \frac{u_s^{i*}(1)}{(R^* - 1)}\right) - 2\mathrm{A}_2 r_2^*\left(\frac{u_s^{m*}(r^*)}{(R^* - r^*)} - \frac{u_s^{m*}(r_2^*)}{(R^* - r_2^*)}\right). \tag{12}$$

The strain-displacement relation reads [44]:

$$\epsilon_s^{\varrho}(r^*) = \frac{R^*}{R^* - r^*}\frac{\partial u_s^{\varrho *}(r^*)}{\partial s^*} - \frac{u_r^{\varrho *}(r^*)}{R^* - r^*}. \tag{13}$$

The radial displacements ($u_r^{\varrho *}$) are assumed to be small and hence neglected. Differentiating Eq. (12) with respect to s^* and applying the continuity of displacement at the interfaces, $u_s^{i*}(1) = u_s^{f*}$ and $u_s^{m*}(r_2^*) = u_s^{i*}$,

leads to [44, 45]:

$$\frac{\partial^2 \sigma_s^{f*}}{\partial s^{*2}} = -2\mathrm{A}_{1R}[\epsilon_s^i(r^*) - \epsilon_s^f] - 2\mathrm{A}_{2R} r_2^*[\epsilon_s^m(r^*) - \epsilon_s^m(r_2^*)], \tag{14}$$

where $\mathrm{A}_{1R} = \mathrm{A}_1/R^*$ and $\mathrm{A}_{2R} = \mathrm{A}_2/R^*$. Since the radial displacements are assumed to be small, the strains in the radial direction can also be neglected. In other words, we neglect the stresses due to Poisson's effect. Therefore, considering the stresses only along the fiber direction, $\epsilon_s^{f*} = \sigma_s^{f*}, \epsilon_s^{i*} = \sigma_s^{i*}/E^{i*}$ and $\epsilon_s^{m*} = \sigma_s^{m*}/E^{m*}$. Furthermore, based on the shear-lag theory and considering the small diameter of fiber and interphase, strain in the matrix can be estimated as if no fiber and interphase exists [44], i.e., $\epsilon_s^m(r_3^*) = \epsilon_s^\infty(r_3^* \to \infty) = \sigma_s^{f*}/(E^{m*} r_3^{*2})$. Also, from the compatibility of strains at the interface between interphase and matrix, $\epsilon_s^i(r_2^*) = \epsilon_s^m(r^* = r_2^*) = \sigma_s^{f*}/(E^{m*} r_2^{*2})$. Therefore, Eq. (14) simplifies to:

$$\frac{\partial^2 \sigma_s^{f*}}{\partial s^{*2}} = -2\mathrm{A}_{1R}\left(\frac{\sigma_s^{i*}}{E^{i*}} - \sigma_s^{f*}\right) - 2\mathrm{A}_{2R} r_2^*\left(\frac{\sigma_s^{f*}}{E^{m*} r_3^{*2}} - \frac{\sigma_s^{f*}}{E^{m*} r_2^{*2}}\right). \tag{15}$$

Equation (15) is differentiated twice to obtain the fourth order governing differential equation:

$$\frac{d^4 \sigma_s^{f*}}{ds^{*4}} + \mathrm{T}_2 \frac{d^2 \sigma_s^{f*}}{ds^{*2}} + \mathrm{T}_1 \sigma_s^{f*} = 0, \tag{16}$$

where T_1 and T_2 are given by:

$$\mathrm{T}_1 = \frac{2\mathrm{A}_{1R}\mathrm{B}_2\mathrm{A}_{2R} r^*}{E^{i*}}\left[\frac{1}{(R^* - r^*)}\frac{1}{E^{m*} r_3^{*2}} - \frac{1}{(R^* - r_2^*)}\frac{1}{E^{m*} r_2^{*2}}\right], \tag{17a}$$

$$\mathrm{T}_2 = \frac{2\mathrm{A}_{1R}(\mathrm{B}_1 - E^{i*})}{E^{i*}} + \frac{2\mathrm{A}_{2R} r_2^*}{E^{m*}}\left(\frac{1}{r_3^{*2}} - \frac{1}{r_2^{*2}}\right). \tag{17b}$$

The intermediate steps in the derivation of Eq. (16) are given in Appendix B. Solution steps of Eq. (16) to estimate the normal stresses in fiber are derived in Section Appendix C. The relation between the pull-out force and the displacement is estimated in Appendix D.

The normal stress in the interphase (σ_s^{i*}) is estimated using Eq. (B.13) as:

$$\frac{\partial^2 \sigma_s^{i*}}{\partial s^{*2}} = \mathrm{B}_3 \sigma_s^{f*} + \mathrm{B}_2 \frac{\partial^2 \sigma_s^{f*}}{\partial s^{*2}}. \tag{18}$$

where B_3 is given by:

$$\mathrm{B}_3 = \mathrm{B}_2\mathrm{A}_{2R} r_2^*\left[\frac{1}{E^{m*} r_3^{*2}(R^* - r_3^*)} - \frac{1}{E^{m*} r_2^{*2}(R^* - r_2^*)}\right]. \tag{19}$$

The solution steps for the Eq. (18) and the estimation of interfacial stresses are detailed in Appendix E.

2.3. Graded interphases

The stress peaks close to the boundaries of the interfaces (at the edge of the fiber) play a major role in fiber debonding from the matrix. The pull-out can be delayed by reducing the peak stresses. Therefore, the stress peaks can be significantly reduced by tailoring the Young's modulus of the interphase along the radial direction. In this study, the Young's modulus of the interphase is graded along the radial direction, according to: (i) power and (ii) linear laws.

2.3.1. Power law modulus graded interphase

The modulus of interphase is assumed to vary along the radial direction according to a power law:

$$E^{i*}(r) = P r^{*Q} \tag{20}$$

Based on the continuity of the Young's modulus at the interfaces, $r^* = r_1^*$ and $r^* = r_2^*$ yields:

$$Q = \frac{\ln E^{m*} - \ln E^{f*}}{\ln r_2^* - \ln r_1^*} \quad \text{and} \quad P = \frac{E^{f*}}{r_1^{*Q}} = \frac{E^{m*}}{r_2^{*Q}}. \tag{21}$$

Expressing shear modulus of the interphase in terms of its Young's modulus using Eq. (20):

$$G^{i*} = \frac{P r^{*Q}}{2(1 + \nu^i)}. \tag{22}$$

Therefore, the shear strain in Eq. (3) with power law modulus graded interphase can be rewritten using Eq. (22) as:

$$\gamma_{rs}^{i} = \frac{2(1+\nu^{i})\tau_{i1}^{*}}{Pr^{*(Q+1)}}, \tag{23}$$

where the strain displacement relations are expressed in Eq. (4). Combining Eq. (23) with Eqs. (4) and (5):

$$\frac{\partial u_s^{i*}}{\partial r^*} + \frac{u_s^{i*}}{R^* - r^*} - \frac{2(1+\nu^{i})\tau_{i1}^{*}}{P}\frac{1}{r^{*Q+1}} = 0. \tag{24}$$

According to Eq. (21), Q is less than zero when $E^{m*} < E^{f*}$. Therefore, considering Eq. (24) as the ordinary derivative, the solution is estimated as:

$$u_s^{i*}(r^*) = (R^* - r^*)\left(\frac{u_s^{i*}(1)}{(R^*-1)} + \frac{\tau_{i1}^{*}}{G^{i*}R^*}\left[\frac{1}{Q} - \texttt{LerchPhi}\left(\frac{1}{R^*}, 1, Q\right)\right] - \frac{\tau_{i1}^{*}}{G_i^{*}R^*}\left[\frac{1}{Q} - \texttt{LerchPhi}\left(\frac{r^*}{R^*}, 1, Q\right)\right]\right), \tag{25}$$

The details of derivation are given in Appendix A. The interfacial shear stress is estimated by rearranging Eq. (25):

$$\tau_{i1}^{*} = \mathrm{A}_4\left[\frac{u_s^{i*}(r^*)}{(R^*-r^*)} - \frac{u_s^{i*}(1)}{(R^*-1)}\right], \tag{26}$$

where A_4 is given by:

$$A_4 = \frac{G^{i*}R^*}{\left[\texttt{LerchPhi}\left(\frac{r^*}{R^*}, 1, Q\right) - \texttt{LerchPhi}\left(\frac{1}{R^*}, 1, Q\right)\right]}. \tag{27}$$

Hence, following the similar procedure outlined in section 2.2, the fourth order governing differential equation with power law modulus graded interphase is derived as:

$$\frac{d^4\sigma_s^{f*}}{ds^{*4}} + \mathrm{T}_4\frac{d^2\sigma_s^{f*}}{ds^{*2}} + \mathrm{T}_3\sigma_s^{f*} = 0, \tag{28}$$

where T_3 and T_4 are estimated as:

$$\mathrm{T}_3 = \frac{2\mathrm{A}_{4R}\mathrm{B}_2\mathrm{A}_{2R}r^*}{E^{i*}}\left[\frac{1}{(R^*-r^*)}\frac{1}{E^{m*}r_3^{*2}} - \frac{1}{(R^*-r_2^*)}\frac{1}{E^{m*}r_2^{*2}}\right], \tag{29a}$$

$$\mathrm{T}_4 = \frac{2\mathrm{A}_{4R}(\mathrm{B}_1 - E^{i*})}{E^{i*}} + \frac{2\mathrm{A}_{2R}r_2^*}{E^{m*}}\left(\frac{1}{r_3^{*2}} - \frac{1}{r_2^{*2}}\right). \tag{29b}$$

Equation (28) is solved similar to that of Eq. (16).

2.3.2. Linearly modulus graded interphase

Considering linear variation of the modulus of interphase along the radial direction,

$$E^{i*}(r) = a + br^* \tag{30}$$

Based on the continuity of the Young's modulus at the interfaces, $r^* = r_1^*$ and $r^* = r_2^*$:

$$a = \frac{r_i^*}{r_i^* - r_f^*}E^{f*} - \frac{r_f^*}{r_i^* - r_m^*}E^{m*} \quad \text{and} \quad b = -\frac{E^{f*} - E^{m*}}{r_i^* - r_f^*} \tag{31}$$

Therefore, the shear strain given by Eq. (3) with linearly modulus graded interphase can be expressed as:

$$\gamma_{rs}^{i} = \frac{2(1+\nu^{i})\tau_{i1}^{*}}{(a+br^*)r^*}. \tag{32}$$

Following the similar procedure in Section 2.3.1, the interfacial shear stresses can be written as:

$$\tau_{i1}^{*} = \mathrm{A}_5\left[\frac{u_s^{i*}(r^*)}{(R^*-r^*)} - \frac{u_s^{i*}(1)}{(R^*-1)}\right]. \tag{33}$$

where A_5 is given by:

$$A_5 = \frac{1}{2(1+\nu^i)\left[\frac{\tanh^{-1}\left(\frac{(R^*b-a)}{\sqrt{(a-R^*b)(aR^*-b)}}\right)}{\sqrt{(a-R^*b)(aR^*-b)}} - \frac{\tanh^{-1}\left(\frac{(R^*b-a)r^*}{\sqrt{(a-R^*b)(aR^*r^*-br^{*3})}}\right)}{\sqrt{(a-R^*b)(aR^*r^*-br^{*3})}}\right]}. \tag{34}$$

The normal stresses in the fiber and hence the shear stresses are estimated following the similar procedure outlined in Section 2. The developed methodology has been extended to study the mechanics of straight fiber pull-out in a fiber, interphase and matrix system. Detailed steps of estimating stresses in the fiber, interphase and matrix are given in Appendix F.

3. Interfacial debonding and sliding

According to the maximum shear stress theory, debonding occurs when the interfacial shear stress is more than the interfacial shear strength (τ_s^*), i.e., $\tau_{i1}^* \geq \tau_s^*$. Different stages of the fiber pull-out process are shown in Fig. 2. In the first stage (Fig. 2(a)), fiber is considered to be fully bonded to the interphase. Increasing the pulling force (P_f) on the fiber leads to debonding. Therefore, stage II corresponds to a partially debonded situation, where (L-z) and z are the debonded and bonded lengths, respectively, see Fig. 2(b). Finally, the fully debonded stage III is reached as shown in Fig. 2(c).

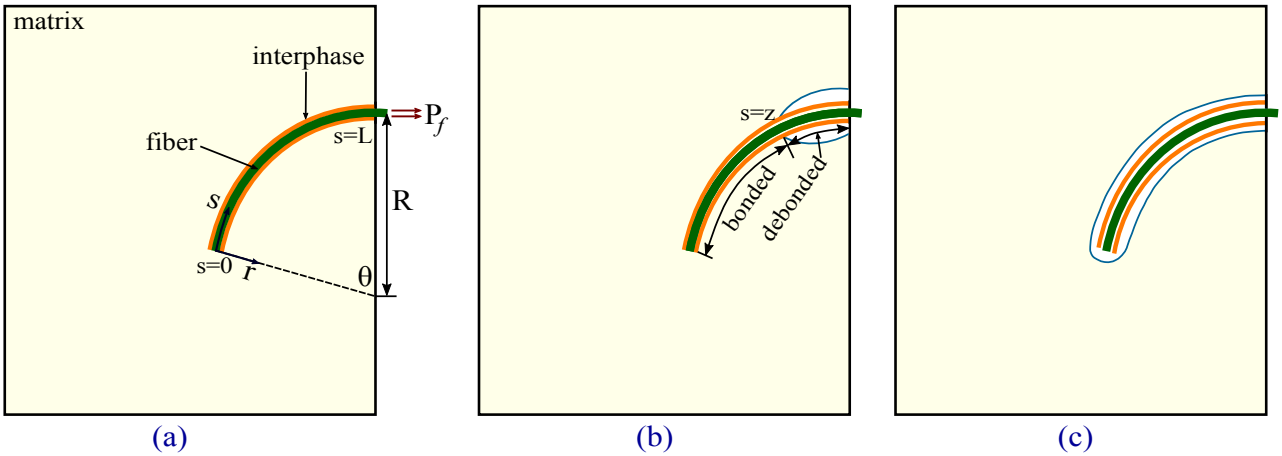

Figure 2: Three different stages of the fiber pull-out: (a) Stage I, fiber perfectly bonded to the surrounding interphase and so is the interphase with matrix. (b) Stage II, partially debonded fiber. The length of the debonded fiber is $(L-z)$. (c) Stage III, completely debonded fiber.

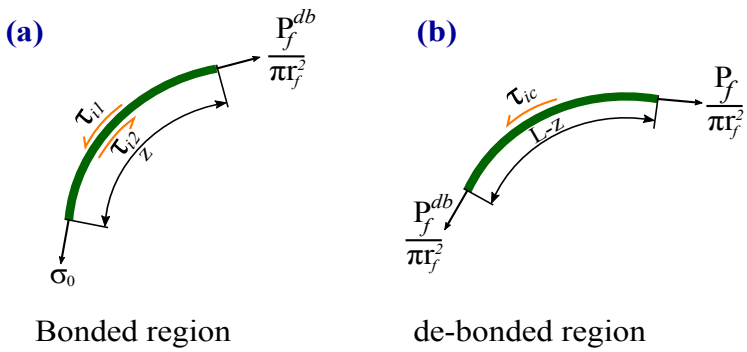

Figure 3: Equilibrium of forces in the (a) bonded and (b) de-bonded regions.

Consider the force equilibrium of debonded and boned regions as shown in Fig. 3(a) and (b), respectively. The total applied load on the fiber P_f can be expressed as $P_f = \pi r_f^2 \sigma_s^f$, where σ_s^f is the axial stress in the fiber at $s = L$. Let P_f^{db} is the load in the fiber at $s = (L-z)$. Therefore, $P_f^{db} = \pi r_f^2 \sigma_s^{f\,db}$, where $\sigma_s^{f\,db}$ is the axial stress in the fiber at $s = (L-z)$. Let τ_{ic} be the constant interfacial friction stress between the fiber and interphase, resisting the applied load, see Fig. 3(a). The interfacial shear stresses τ_{i1} and τ_{i2} acts in the opposite direction

of pull-out force as shown in Fig. 3(b). Considering the equilibrium of forces in the debonded and bonded regions:

$$\mathrm{P}_f^* - \mathrm{P}_f^{db*} = 2\tau_{ic}(L^* - z^*), \tag{35}$$

Therefore, the normal stress in the fiber can be estimated from

$$\sigma_s^{f*} = \mathrm{P}_f^{db*} + 2\tau_{ic}(s^* - z^*), \qquad s^* \in (s^*, L^*), \tag{36}$$

At the boundary between the bonded and debonded parts, i.e. at $s^* = z^*$, $\tau_i^* = \tau_s^*$. Therefore, in the perfectly bonded region the stress expression derived in the previous section is used. Whereas, in the debonded region the interfacial frictional stresses (τ_{ic}) resists the pull-out force [45].

4. Results and discussion

The developed methodology has been used to estimate the stresses in a curved fiber pull-out problem of a three phase system. In this section, results from the fiber pull-out studies are summarized. Results estimated from the present analytical model are validated by comparing them with the numerical results obtained from finite element analysis performed using ABAQUS/standard FEA. Furthermore, the influence of graded interphase on stress transfer is studied by comparing the results from the three phase system with the results from the two phase system (a curved fiber embedded in a matrix (FM) [44]).

A three phase system with a fiber of radius 1.5 nm, surrounded by an interphase of radius 1.7 nm, and a matrix of dimensions $30 \times 40 \times 5$ nm^3 is analysed. The material and geometric properties used in the present study are summarized in Table 1. For convenience, normalized quantities are used in all the calculations. Both actual and normalized quantities are listed in Table 1.

R (nm)	L (nm)	r_f (nm)	r_i (nm)	E_f (Pa)	E_m (Pa)
20.2	32.23	1.5	1.7	1e12	1e9
σ_0^*	L^*	P_f^*	r_m^*	G_m^*	E_m^*
1e-9	21.49	2.5e-3	20	3.7e-4	1e-3

Table 1: Material and geometric properties of the three phase system.

4.1. Axial stresses

The distribution of the normalized axial stress (σ_f^*) over normalized projected length along the fiber axis (s direction), is plotted in Fig. 4. In each subplot of Fig. 4, specific case for which the results are extracted is highlighted through a schematic in the inset. The stresses are extracted along the fiber length. Variation of the normalized axial stresses for FM and FIM systems are shown in Fig. 4(a) and (b), respectively. A comparison of axial stresses in two and three phase systems is shown in Fig. 4(c). Analytical results considering the linear and power law variation of modulus in the interphase region, are compared to the results of the ungraded system in Fig. 4(d).

A comparison of the normalized normal stresses in the fiber in a two phase system from the analytical [44] and finite element models is shown in Fig. 4(a). Based on Fig. 4(a), the analytical results are observed to satisfy the imposed traction boundary conditions at the top ($z = L$) and bottom ($z = 0$) fiber surfaces. This is verified by noticing the value of the normalized axial stress, (i) at $z = L$ is 2.5×10^{-3}, which is equal to the prescribed stress (σ_0) on the fiber top end and (ii) at $z = 0$ is almost zero, satisfying the zero stress condition at the bottom of the fiber. Similar trend is observed in the three phase system (see Fig. 4(b)) as well. A close agreement of the analytical and numerical results of the two phase system is noticed in Fig. 4(a).

In order to validate the analytical results of the three phase system, a three dimensional (3D) finite element model was created using the ABAQUS/standard FEA. The geometric and material properties summarized in Table 1 are used in the FE analysis as well. A summary of the finite element analysis is presented in Fig. 5. Figure 5(a) shows the geometry and boundary conditions of the fiber along with the interphase embedded in a matrix. Pressure load is prescribed on the fiber cross section at the end $s = L$, whereas the top, bottom and left edges of the matrix are completely constrained. The geometry is discretized using the 'tetrahedron' elements. The present numerical model consists of 204669 elements, 320395 nodes and 961185 degrees of freedom in total. The final number of elements are arrived after the mesh convergence studies conducted following [31]. The deformed configuration at the end of the simulation is shown in Fig. 5(b). Figure 5(b) highlights the geometry and location of the fiber in the deformed configuration.

Variation of the normalized normal stresses in the fiber along the fiber direction in a three phase system are plotted in Fig. 4(b). Distribution of the normal stresses in the fiber estimated from the numerical analysis is shown in Fig. 5(c). The stresses along the fiber axis from the analytical and numerical models are compared

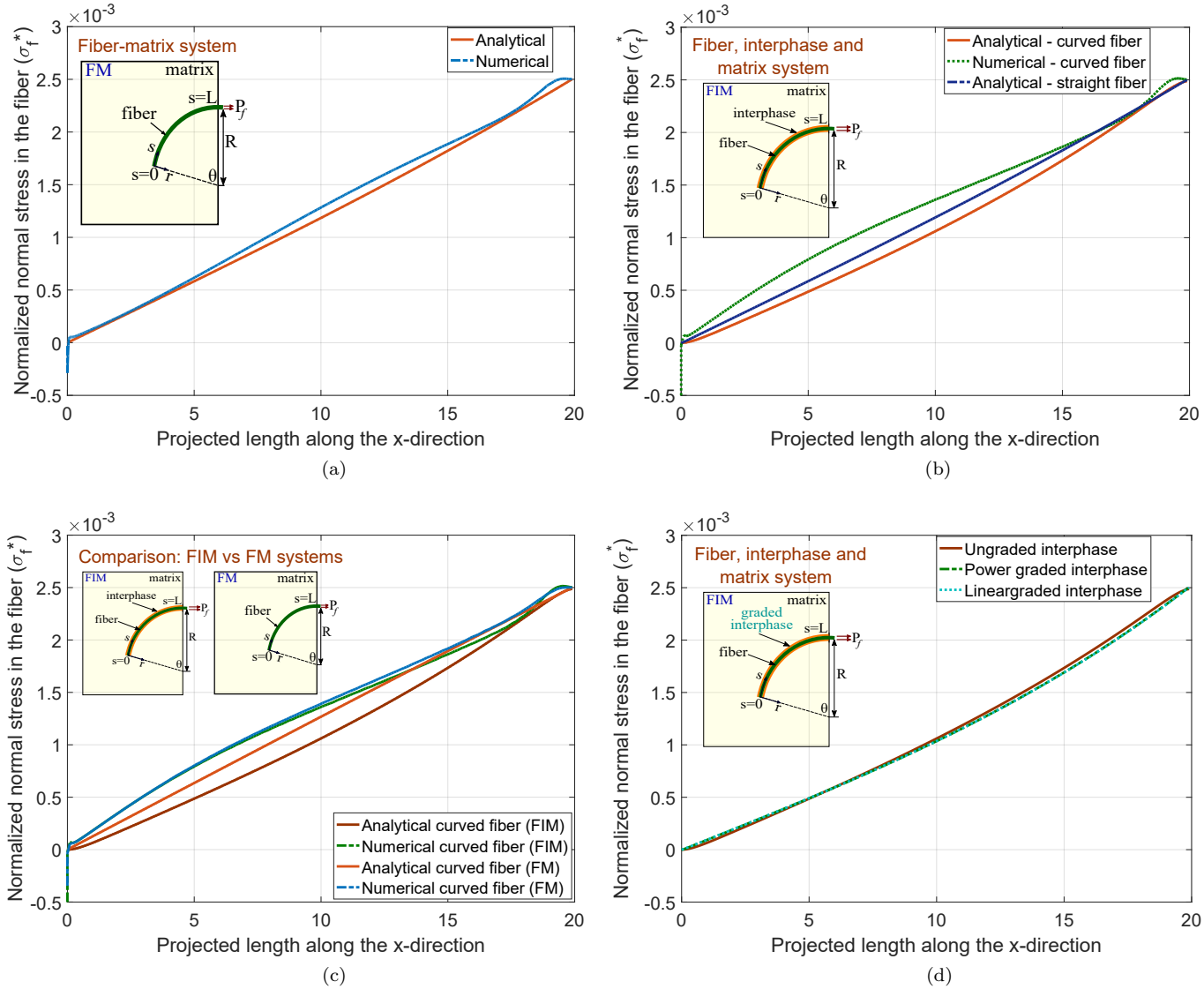

Figure 4: Variation of the normalized axial stresses in the fiber with the normalized length along the s-direction: (a) comparison of analytical and numerical results for a two phase system, (b) axial stresses in the fiber in a three phase system, estimated from the analytical models of a straight and curved fiber, compared to the numerical results, (c) comparison of analytical and numerical results of two and three phase systems and (d) the influence of grading on fiber normal stresses in a three phase system.

in Fig. 4(b). Furthermore, Fig. 4(b) also shows the axial fiber stresses considering a straight fiber in a three phase system. For the given system, the normalized normal stress in the curved fiber in a three phase system is observed to be lower compared to that of the straight fiber. The modeled length of the straight fiber is equal to length of the curved fiber along the fiber axis (s direction). The bonded area of the curved fiber is more than the area that of the straight fiber. As a result, for a given loading, the resistance is more in a curved fiber, leading to lower stresses than that of a straight fiber. In other words, higher forces are required to pull-out a curved fiber from the matrix. Therefore, curved fibers are recommended to enhance the mechanical properties of polymer nano-composites for structural applications.

Separate analysis with and without interphase is carried out to pin-point the influence of interphase in reducing the stress peaks. The normalized axial fiber stresses in two and three phase systems from the analytical and numerical models are compared in Fig. 4(c). Based on Fig. 4(c), the axial stresses in the two phase system are higher compared to the three phase system. This is evident from both analytical and numerical results. The normal stresses in the fiber are transmitted to the matrix through shear stresses in the interlayer. Distribution of the normal stresses in the fiber, interphase and fibre-interphase interface are shown in Fig. 5(c), (e) and (g), respectively. Similarly, distribution of the shear stresses in the fiber, interphase and fibre-interphase are shown in Fig. 5(d), (f) and (h), respectively. Comparing the normal and shear stresses in Fig. 5(c)-(h), the point of highest stress is observed to be located in the fiber. Therefore, fiber is the most stressed member in the composite. Furthermore, comparing the pattern of normal stresses in the fiber and interphase in Fig. 5(c) and (e), the normal stresses are higher towards the loading end, happening after a smooth transfer from the fiber

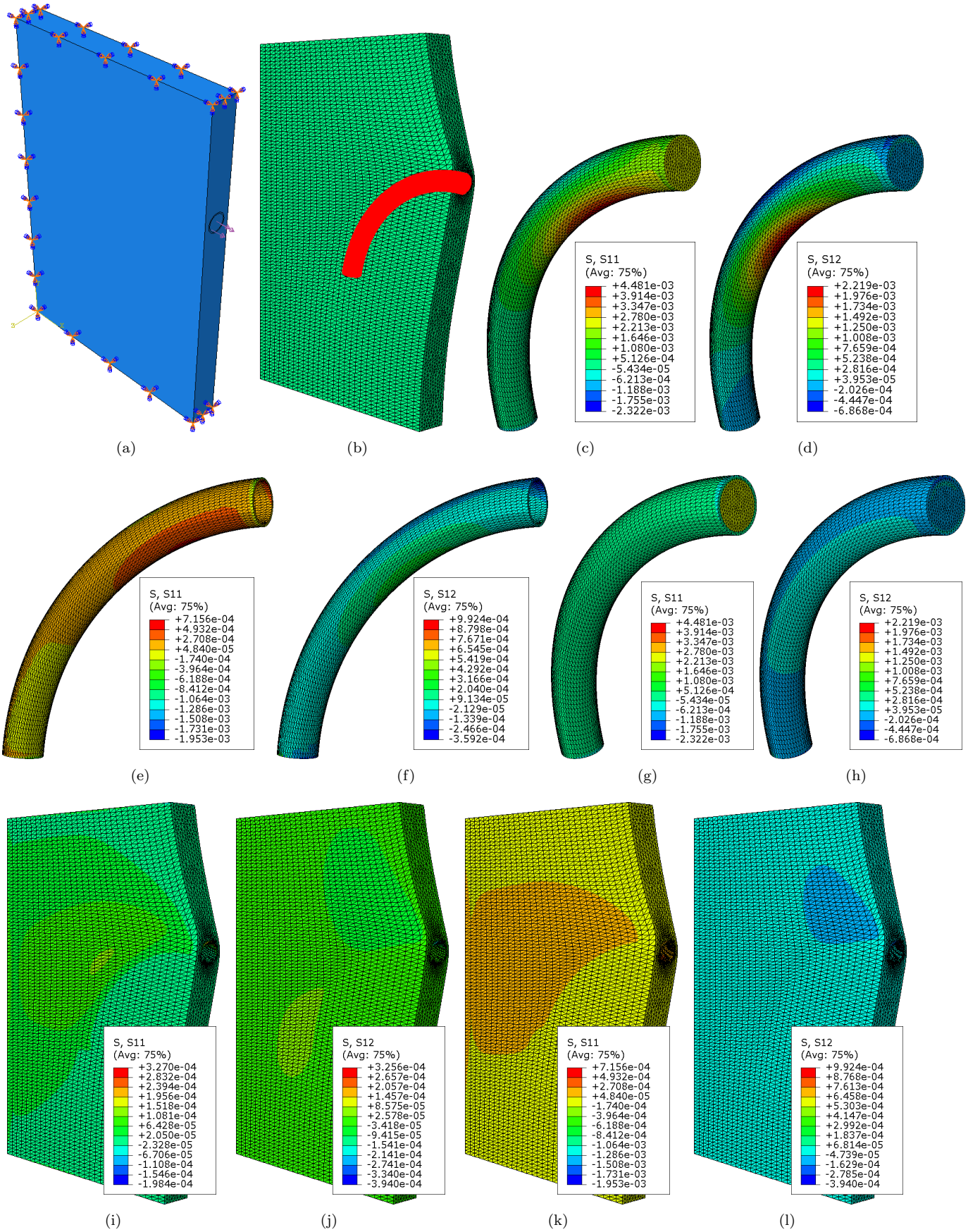

Figure 5: Results of the finite element analysis of curved fiber pull-out in a three phase system. (a) Geometry along with the loading and boundary conditions. Pressure load is prescribed on the fiber cross section, whereas the top, bottom and left edges of the matrix are completely constrained. (b) Deformed configuration highlighting the location and geometry of the fiber. Distribution of the normal stress (σ_{11}) in the (c) fiber, (e) interphase, (g) fiber and interphase, (i) matrix and (k) matrix and interphase. Similarly, distribution of the shear stress (σ_{12}) in the (d) fiber (f) interphase, (h) fiber and interphase, (j) matrix and (l) matrix and interphase.

to the interphase. This is further confirmed by the distribution of the normal stresses in fiber and interphase together in Fig. 5(g). In the similar lines, a smooth transfer of shear stresses between the fiber and interphase is noticed in Fig. 5(h) aswell. Therefore, the interphase aids in reducing the stress peaks and hence smooth transfer of stresses between the fiber and matrix.

Variation of the normalized normal stresses in the fiber in the presence of graded interphase with power law and linear modulus tailoring is shown in Fig. 4(d). The influence of grading on the fiber normal stress is insignificant. The Young's modulus of the interphase is graded along the radial direction according to power and linear laws, as mentioned in Eqs. (20) and (30). The fiber transfers the external loads through normal stresses. The interphases are engineered to smoothly transfer the axial stresses in the fiber to the matrix, by reducing the stress peaks at the interfaces. Therefore, axial stresses in the fiber are not influenced by the graded interphases.

4.2. Interfacial shear stresses

Figure 6 is dedicated to the comparison of normalized first interfacial stress (τ_{i1}) between the fiber and interphase. Interfacial stresses in a two phase system from the analytical [44] and numerical models are compared

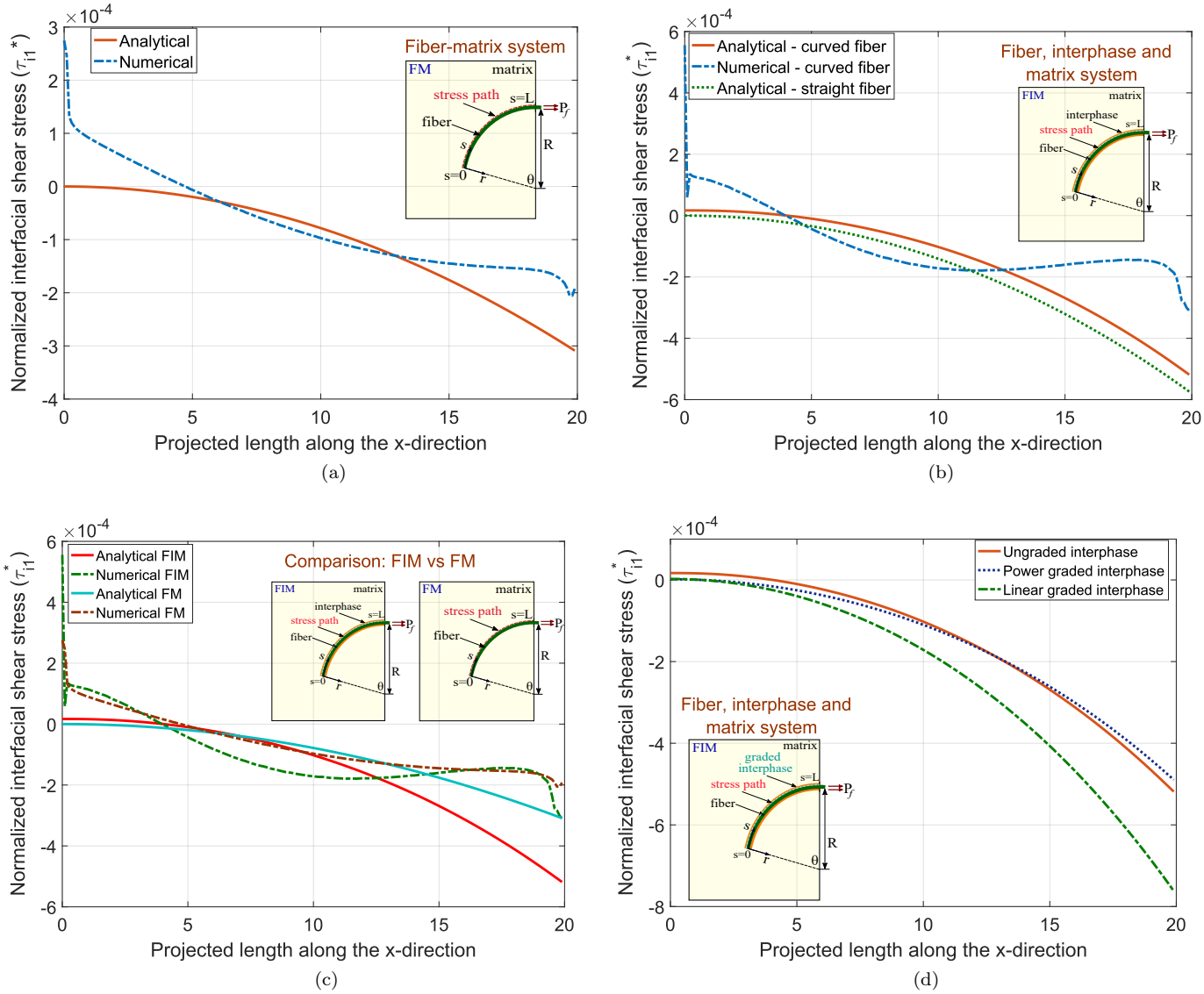

Figure 6: Variation of first interfacial shear stress (τ_{i1}^*) with the normalized projected length along the x-direction; (a) comparison of results of a two phase system from finite element analysis and analytical model, (b) interfacial stresses in a three phase system estimated from analytical models of a straight and curved fiber, compared to the numerical results, (c) comparison of analytical and numerical results of two and three phase systems and (d) influence of grading on interfacial shear stresses in a three phase system.

in Fig. 6(a). In the analytical model, the shear stress is enforced to be 'zero' at the embedded end of the fiber. Whereas, no such conditions are enforced in the finite element analysis. In analytical model, the embedded length of the fiber is assumed to be large enough for shear dominated load transfer. For the given geometric,

material and loading conditions, FE model should reveal zero shear stress at the embedded end if the length of embedment is large enough. This is the reason for the difference in the amplitude of τ_{i1} at $s = 0$ in Fig. 6(a). A smooth variation of τ_{i1} of the analytical results are observed, as compared to the numerical results. In general, mesh size and the contact between the fiber and interface in the finite element analysis will influence the results. However, the present results are in good agreement, particularly in the middle of the domain. Comparison of τ_{i1} estimated in a three phase system from analytical model with straight and curved fibers, with the results from FE analysis are shown in Fig. 6(b). Based on Fig. 6(b), interfacial stresses in the curved fiber are higher in the curved fiber compared to the straight fiber. This is because of the larger contact area in case of curved fiber, compared to the straight fiber.

Distribution of the normal stresses and shear stresses in the matrix is shown in Fig. 5(i) and (j), respectively. Similarly, Fig. 5(k) and (l) shows the distribution of the normal and shear stresses in the matrix including the interphase. Comparing Fig. 5(i) and (k), the maximum amplitude of the normal stress is lower in the matrix alone as compared to the matrix including the interphase. Similarly, comparing Fig. 5(j) and (l), the maximum amplitude of the shear stress is lower in the matrix alone as compared to the matrix including the interphase. Therefore, the stresses in matrix are the lowest when compared to the stresses in the fiber and interphase. This indicates a complete transfer of fiber stresses to the interphase and hence to the matrix.

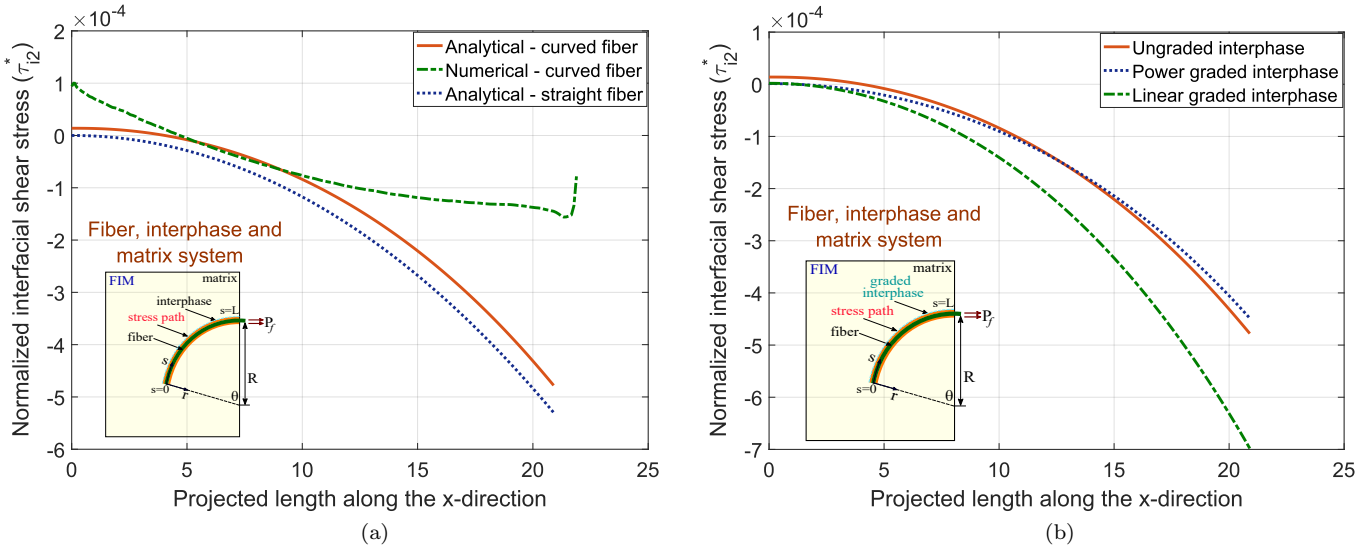

Figure 7: Comparison of interfacial shear stress (τ^*_{i2}) between the interphase and matrix in a three phase system; (a) with straight, curved fibers and the FE results and (b) with graded and ungraded interphases.

Comparison of τ_{i1} in two phase and three phase systems is shown in Fig. 6(c). Influence of the interphase in three phase system can be noticed based on the lower stresses at the interphase as shown in Fig. 6(c). The influence of grading the interphase based on the linear and power laws is shown in Fig. 6(d). From Fig. 6(d), a linearly graded interphase shows the lowest interfacial stresses at the loaded end. On the other hand, the influence of a power graded interphase is insignificant compared to the ungraded interphase. Interfacial stresses between the interphase and matrix in a three phase system are shown in Fig. 7. According to Fig. 7(a), the magnitude of τ_{i2} in case of the curved fiber is higher compared the straight fiber. Influence of the graded interphase according to the linear law is significant compared to ungraded and power graded interphase, as shown in Fig. 7(b).

Results from the analytical model of a three phase system with straight fiber are plotted in Fig. 8. Comparison of the normalized normal stresses and interfacial stress between the fiber and interphase (τ_{i1}) with ungraded, power law graded and linearly graded interphases are shown in Figs. 8(a) and (b), respectively. As observed in the case of curved fiber, the normal stresses in the straight fiber are also not influenced by the graded interphases. According to Fig. 8(b), both power and linear grading are observed to be significantly influencing the interfacial stresses, τ_{i1}.

A parametric study has been carried out to examine the influence of various parameters on the pull-out behaviour of curved fiber for perfectly bonded case. The parameters of interest include the fiber normalized radius of curvature R^*, normalized fiber length L^* and the fiber axial stress at the embedded end σ^*_0. Figures 9 and 10 summarizes the parametric studies through the variation of the pull-out force as a function of the normalized displacements. The load displacement diagram as the fiber is pulled out from the matrix is shown in Figure 9(a). The point of deboding is indicated by the maximum value of the pull-out force [45], see the inset picture in Figure 9(a). The dobonding is observed to be stable until the maximum pull-out force, beyond which the failure is catastrophic where the load transfer mechanics between fiber and interphase happens

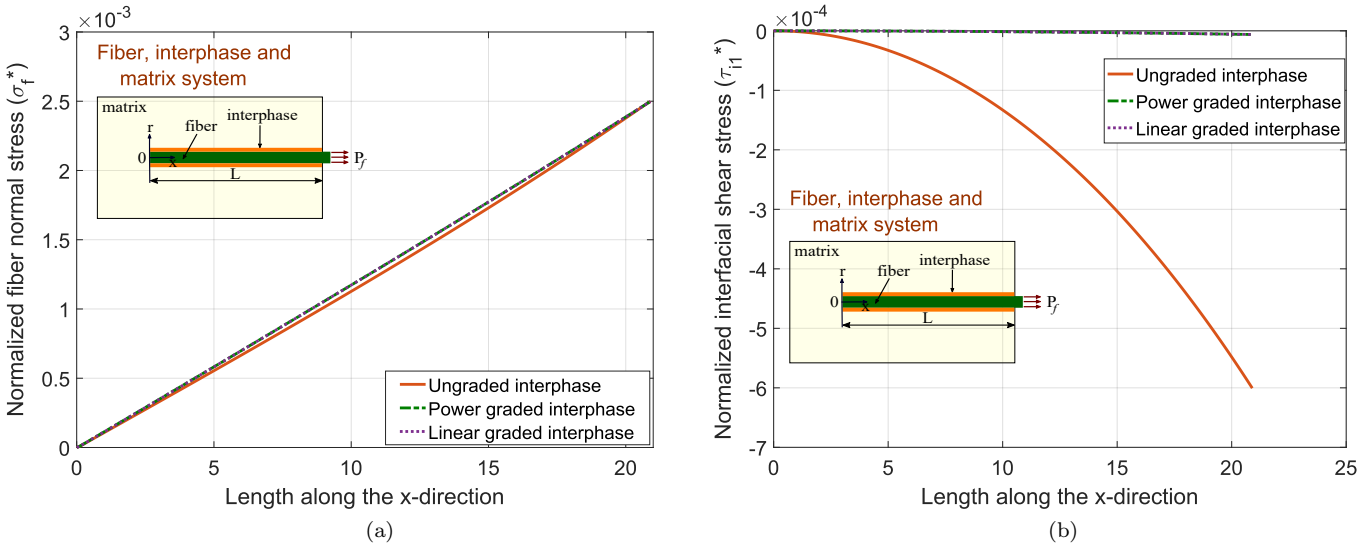

Figure 8: Analysis of a three phase system with straight fiber. (a) Comparison of the normalized normal stresses with ungraded, power graded and linearly graded interphases. (b) Comparison of interfacial stress between the fiber and interphse (τ_{i1}).

predominantly through frictional forces in the debonded region [45]. Figure 9(b) shows the variation of the pull-out force at different radius of curvature for a normalized fiber length (L^*) equal to 20. The displacements are purely due to fiber elongation, as perfect bonding between the fiber, interphase and matrix is assumed with no relative displacement. The considered fiber length in the analysis is smaller compared to typical nanotube length observed in practical applications, which is of the order of hundreds of nano meters. This is because the present focus is only on a curved segment of the nanotube. Based on Fig. 9(b) the variation is observed to be linear and slope is increasing with the radius of curvature. The results indicate that for the given fiber length, the pull-out force required to displace the fiber by a certain distance increases with the increase in the radius of curvature. When only the bonded condition prevails the load-displacement curve is terminated when the debonding starts due to interfacial stress stress reaching a critical value.

Variation of the pull-out force with the normalized displacements for different fiber lengths is shown in Fig. 9(c). The slope of the curves is observed to be decreasing with increasing fiber length. Hence, the force required to pull the fiber for a given displacement will be decreasing with increasing fiber length. In other words, for a given force, the displacement increases with increase in length. Therefore, with increasing L^* and R^* the debonding initiation force is decreasing. The reason being, in case of short fibers, the fibers are perfectly anchored in the matrix and hence the bonding between the fiber and in the interphase can be ensured perfect. As a result, the pull-out happens with small debond regions and occurs suddenly like a brittle failure, when the pull-out force force reaches a threshold. However, in the case of long fibers the debonding happens over a significant period of time before the fiber is pulled out of the matrix. Small forces are required to cause the debonding of fiber from the interphase, as compare to the pull-out forces. In the limit the straight fiber requires the lowest pull-out force to initiate the debonding. In other words, for the given pull-out force the interfacial shear stress in the curved fiber is smaller than that of the straight fiber. Influence of σ_0 on the pull-out force is plotted in Fig. 9(d). Increasing σ_0 from 1e-9 to 1e-4 , increases the end stresses, which finally leads to higher debond initiation force. A non-zero displacement for a zero pull-out force at large end stresses is because of the fiber elongation from residual stresses. However, from Fig. 9 both σ_0^* and R^* has the minimum effect in the bonded stage, whereas, the influence of L^* is significant. Therefore, long curved fibers requires higher debond initiation forces, leading to improved toughness of the PNC.

Effect of graded interphases on the pull-out force are revealed in Fig. 10. Based on Fig. 10(b) the influence of radius of curvature on the pull-out force with graded interphases is minimum. Whereas, significant increase in the pull-out force with graded interphases for the given fiber length can be noticed in Fig. 10(c). The stiffness of the interphase gradually increases from the fiber surface towards the matrix surface. Therefore, graded interphases enhances the shear stress transfer and improves the strength of PNC.

5. Conclusions

An analytical model has been proposed in this paper, to study the micromechanics of stress transfer in a curved fiber pull-out test. Closed form expressions are derived to estimate the normal and shear stresses in fiber, interphase and matrix system, based on the shear-lag theory.

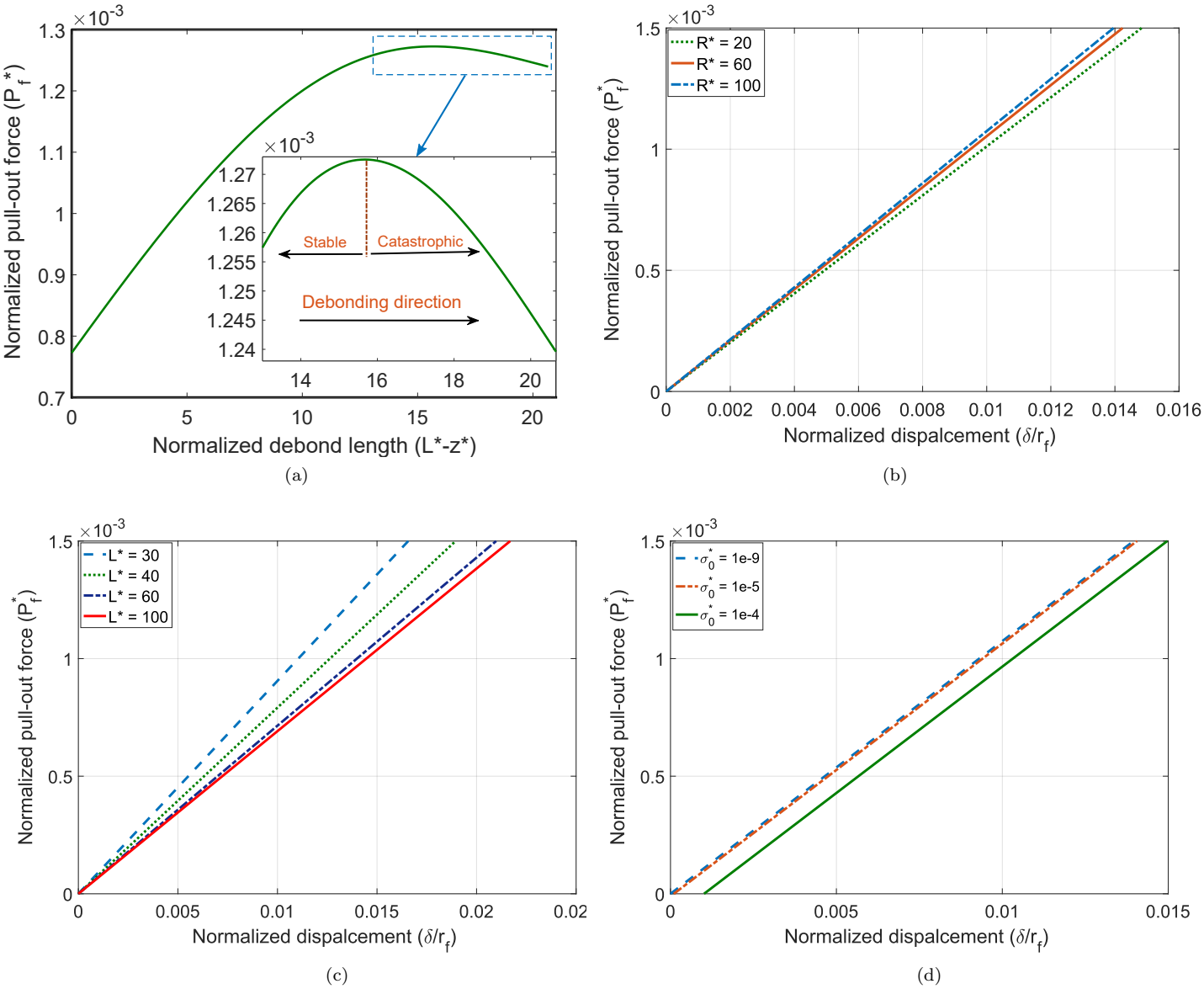

Figure 9: Pull-out force as a function of displacement. Variation of the pull-out force as a function of (a) radius of curvature of fiber at normalized fiber length equal to 20, (b) fiber length at normalized fiber radius equal to 20 and (c) σ_0 at normalized fiber length and radius of 20.

The developed methodology has been applied to estimate the constituent stresses in a curved fiber pull-out test. Analytical results are validated by comparing the axial and shear stresses in the fiber and interphase with the numerical results. A close agreement of the results from the analytical and numerical models has been observed.

Furthermore, to drastically reduce the stress peaks across the interfaces, the modulus of the interphase is graded along the radial direction, according to power and linear laws. Linearly graded interphases are noticed to be efficient in reducing the stresses. The developed methodology has been extended to study the stress transfer mechanics in a straight fiber pull-out test. Because of the availability of more area of resistance in case of a curved fiber, the stresses in curved fiber are observed to be on the lower side, compared to the stresses in a straight fiber. Therefore, curved fibers are recommended to enhance the mechanical properties of polymer nano-composites for structural applications.

Acknowledgements

The authors acknowledge funding through the cooperative agreement between the Masdar Institute of Science and Technology (Masdar Institute), Abu Dhabi, UAE and the —

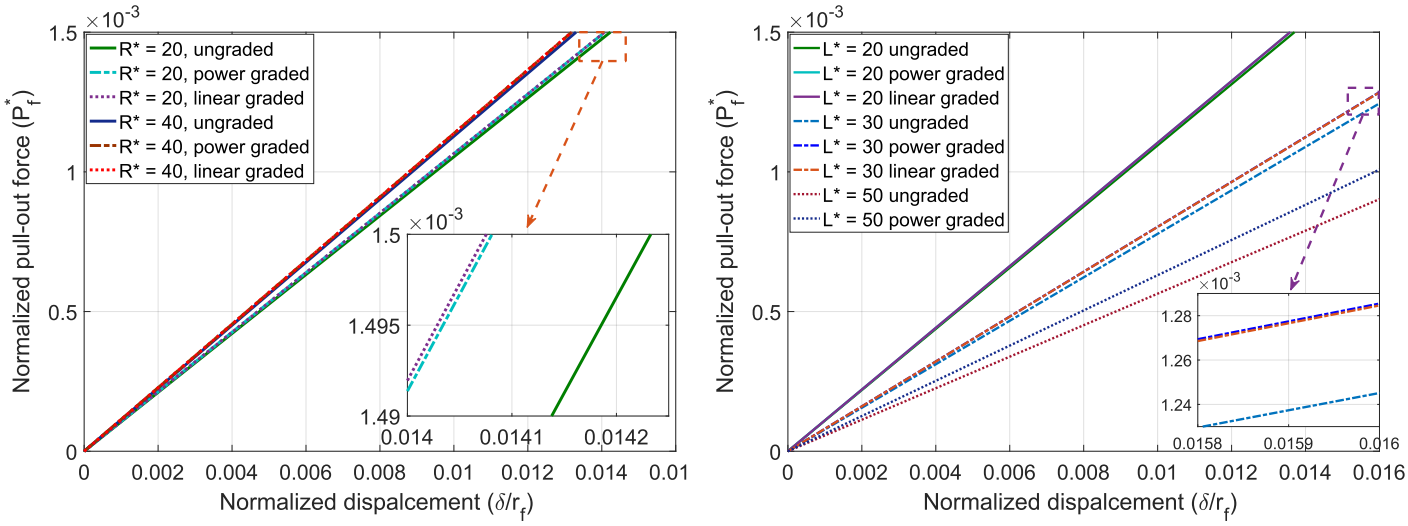

(a) (b)

Figure 10: Influence of graded interphases on the pull-out force. Pull-out force at different (a) radius of curvature and (b) fiber lengths. Power and linear grading of the grading laws are compared to the ungraded interphase.

References

[1] JK Wells and PWR Beaumont. Debonding and pull-out processes in fibrous composites. *Journal of Materials Science*, 20(4):1275–1284, 1985.

[2] C Ageorges, T. Schüller, and B. Lauke. Single-fibre broutman test: fibre-matrix interface transverse debonding. *Composites: Part A*, 30:1423–1434, 1999.

[3] L Yang and JL. Thomason. Interface strength in glass fibre-polypropylene measured using the fibre pull-out and microbond methods. *Composites: Part A*, 41:1077–1083, 2010.

[4] S Tamrakar, BZ Haque, and JW. GillespieJr. High rate test method for fiber-matrix interface characterization. *Polymer Testing*, 52:174–183, 2016.

[5] S Nuriel, A Katz, and HD. Wagner. Measuring fiber-matrix interfacial adhesion by means of a drag-out micromechanical test. *Composites: Part A*, 36:33–37, 2005.

[6] F Gardea, B Glaz, J Riddick, DC Lagoudas, and M. Naraghi. Identification of energy dissipation mechanisms in cnt-reinforced nanocomposites. *Nanotechnology*, 27:105707, 2016.

[7] M Braginsky and CP. Przybyla. Simulation of crack propagation/deflection in ceramic matrix continuous fiber reinforced composites with weak interphase via the extended finite element method. *Composite Structures*, 136:538–545, 2016.

[8] D Notta-Cuvier, F Lauro, and B. Bennani. Modelling of progressive fibre/matrix debonding in short-fibre reinforced composites up to failure. *International Journal of Solids and Structures*, 66:140–150, 2015.

[9] M Nishikawa, T Okabe, N Takeda, and WA. Curtin. Micromechanics of the fragmentation process in single-fiber composites. *Modelling and Simulation in Material Science and Engineering*, 16:055009, 2008.

[10] P Feillard, G Désarmot, and JP. Favre. Theoretical aspects of the fragmentation test. *Composites Science and Technology*, 50:265–279, 1994.

[11] AP Awasthi, DC Lagoudas, and DC. Hammerand. Modeling of graphene-polymer interfacial mechanical behavior using molecular dynamics. *Modelling and Simulation in Material Science and Engineering*, 17:015002, 2009.

[12] YB Lu, QS Yang, XQ He, and KM. Liew. Modeling the interfacial behavior of carbon nanotube fiber/polyethylene composites by molecular dynamics approach. *Computational Materials Science*, 114:189–198, 2016.

[13] F Danzi, D Fanteria, E Panettieri, and M. Palermo. A numerical micro-mechanical study of the influence of fiber-matrix interphase failure on carbon/epoxy material properties. *Composite Structures*, 159:625–635, 2017.

[14] S Sockalingam, M Dey, JW GillespieJr, and M. Keefe. Finite element analysis of the microdroplet test method using cohesive zone model of the fiber/matrix interface. *Composites Part A: Applied Science and Manufacturing*, 56:239–247, 2014.

[15] T Okabe, N Takeda, Y Kamoshida, M Shimizu, and WA. Curtin. A 3d shear-lag model considering micro-damage and statistical strength prediction of unidirectional fiber-reinforced composites. *Composites Science and Technology*, 61:1773–1787, 2001.

[16] Q Wu, M Li, Y Gu, Y Li, and Z. Zhang. Nano-analysis on the structure and chemical composition of the interphase region in carbon fiber composite. *Composites: Part A*, 56:143–149, 2014.

[17] RM Christensen and KH. Lo. Solutions for effective shear properties in three phase sphere and cylinder models. *Journal of the Mechanics and Physics of Solids*, 27(4):315–330, 1979.

[18] W Wu, E Jacobs, I Verpoesta, and J. Varna. Variational approach to the stress-transfer problem through partially debonded interfaces in a three-phase composite. *Composites Science and Technology*, 59:519–535, 1999.

[19] S Rjafiallah, S Guessasma, and H. Bizot. Effect of surface etching on interphase and elastic properties of a biocomposite reinforced using glass-silica particles. *Composites Science and Technology*, 70:1272–1279, 2010.

[20] Y Yao, S Chen, and P. Chen. The effect of a graded interphase on the mechanism of stress transfer in a fiber-reinforced composite. *Mechanics of Materials*, 58:35–54, 2013.

[21] T Sabiston, M Mohammadi, M Cherkaoui, J Lévesquec, and K. Inal. Micromechanics for a long fibre reinforced composite model with a functionally graded interphase. *Composites Part B: Engineering*, 84:188–199, 2016.

[22] MA Khan and S. Kumar. A shear-lag model for functionally graded adhesive anchors. *International Journal of Adhesion and Adhesives*, 68:317–325, 2016.

[23] HL. Cox. The elasticity and strength of paper and other fibrous materials. *British Journal of Applied Physics*, 3(3):72, 1952.

[24] JA. Nairn. On the use of shear-lag methods for analysis of stress transfer in unidirectional composites. *Mechanics of Materials*, 26:63–80, 1997.
[25] JA. Nairn. On the use of planar shear-lag methods for stress-transfer analysis of multilayered composites. *Mechanics of Materials*, 33:335–362, 2001.
[26] JA. Nairn. Generalized shear-lag analysis including imperfect interfaces. *Mechanics of Materials*, 13:263–274, 2004.
[27] CH. Hsueh. Interracial debonding and fiber pull-out stresses of fiber-reinforced composites. *Materials Science and Engineering*, A123:1–11, 1990.
[28] CH. Hsueh. Interfacial debonding and fiber pull-out stresses of fiber-reinforced composites, X: with an elastic interfacial coating. *Materials Science and Engineering*, 165:189–195, 1993.
[29] Z Chen and W. Yan. A shear-lag model with a cohesive fibre-matrix interface for analysis of fibre pull-out. *Mechanics of Materials*, 91:119–135, 2015.
[30] WX Chang, H Qing, and CF. Gao. A new theoretical model of the quasistatic single-fiber pull-out problem: A rate-dependent interfacial bond strength. *Mechanics of Materials*, 94:132–141, 2016.
[31] P Upadhyaya and S. Kumar. Micromechanics of stress transfer through the interphase in fiber-reinforced composites. *Mechanics of Materials*, 89:190–201, 2015.
[32] W Wu, I Verpoesta, and J. Varna. A novel axisymmetrix variational analysis of stress transfer into fibres through a partially debonded interface. *Composites Science and Technology*, 58:1863–1877, 1998.
[33] PY Pei, W-X Chang, H Qing, and C-F. Gao. A new theoretical model of the quasistatic single-fiber pullout problem: The energy-based criterion with unloading process. *Composites Science and Technology*, 137:69–77, 2016.
[34] Lianxi Shen and Jackie Li. Homogenization of a fibre/sphere with an inhomogeneous interphase for the effective elastic moduli of composites. *Proceedings of the Royal Society of London A: Mathematical, Physical and Engineering Sciences*, 461(2057):1475–1504, 2005.
[35] H. Qing. A new theoretical model of the quasistatic single-fiber pullout problem: Analysis of stress field. *Mechanics of Materials*, 60:66–79, 2013.
[36] P Upadhyaya and S. Kumar. Pull-out capacity of adhesive anchors: an analytical solution. *International Journal of Adhesion and Adhesives*, 60:54–62, 2015.
[37] R. Sburlati. Stress concentration factor due to a functionally graded ring around a hole in an isotropic plate. *International Journal of Solids and Structures*, 50(22-23):3649–3658, 2013.
[38] S Ben, J Zhao, and T. Rabczuk. A theoretical analysis of interface debonding for coated sphere with functionally graded interphase. *Composite Structures*, 117:288–297, 2014.
[39] Y Jia, Z Chen, and W. Yan. A numerical study on carbon nanotubehybridized carbon fibre pullout. *Composites Science and Technology*, 91:38–44, 2014.
[40] J Karger-Kocsis, H Mahmood, and A. Pegoretti. Recent advances in fiber/matrix interphase engineering for polymer composites. *Progress in Materials Science*, 73:1–43, 2015.
[41] G Pal and S. Kumar. Modeling of carbon nanotubes and carbon nanotube-polymer composites. *Progress in Aerospace Sciences*, 80:33–58, 2016.
[42] L Wang, Y Cui, Q Qin, H Wang, and J. Wang. Helical fiber pull-out in biological materials. *Acta Mechanica Solida Sinica*, 29(3):245–256, 2016.
[43] H Zhang and RC. Yu. Inclined fiber pullout from a cementitious matrix: A numerical study. *Materials*, 9:doi:10.3390/ma9100800, 2016.
[44] X Chen, IJ Beyerlein, and LC. Brinson. Curved-fiber pull-out model for nanocomposites. part 1: Bonded stage formulation. *Mechanics of Materials*, 41:279–292, 2009.
[45] X Chen, IJ Beyerlein, and LC. Brinson. Curved-fiber pull-out model for nanocomposites. part 2: Interfacial debonding and sliding. *Mechanics of Materials*, 41:293–307, 2009.
[46] PM Ajayan, PV Braun, and LS Schadler. *Nanocomposite Science and Technology*. Wiley-VCH Verlag GmbH & Co. KgaA, Weinham, Germany, 2003.
[47] EW Weisstein. *CRC Concise Encyclopedia of Mathematics*. CRC-Press, Chappman & Hall/CRC, 2003.

Appendix A. Solution of differential equations

Consider a first order linear differential equation of the form:

$$\frac{dy}{dx} + p(x)y = q(x). \tag{A.1}$$

Solution of Eq. (A.1) is given by:

$$y = \frac{1}{I(x)} \int I(x)q(x)dx + \frac{C}{I(x)}, \tag{A.2}$$

where

$$I(x) = exp\left(\int p(x)dx\right). \tag{A.3}$$

Therefore, the solution of Eq. (24) can be estimated by evaluating the integral below:

$$\int \frac{dr^*}{(R^* - r^*){r^*}^{Q+1}} = \frac{-\frac{1}{Q} + \texttt{LerchPhi}(\frac{r^*}{R^*}, 1, Q)}{R^* {r^*}^Q} \tag{A.4}$$

where, the `LerchPhi` function is defined as [47]:

$$\texttt{LerchPhi}\left(\frac{r^*}{R^*}, 1, Q\right) = \sum_{n=0}^{\infty} \frac{\left(\frac{r^*}{R^*}\right)^n}{(Q+n)^1} = \sum_{n=0}^{\infty} \frac{\left(\frac{r^*}{R^*}\right)^n}{(Q+n)}, \tag{A.5}$$

such that, $(Q+n) \neq 0$. Hence, the solution of Eq.(24) is given by:

$$u_s^{i*}(r^*) = (R^* - r^*)\left(gr_i(s) - \frac{\tau_{i1}^*}{G^{i*}R^*}\left[\frac{1}{Q} - \texttt{LerchPhi}\left(\frac{r^*}{R^*}, 1, Q\right)\right]\right). \tag{A.6}$$

where $gr_i(s)$ is the arbitrary function defined by the boundary conditions. Considering the interface between the fiber and interphase, $r^* = r_1/r_1 = 1$,

$$u_s^{i*}(1) = (R^* - 1)\left[gr_i(s) - \frac{\tau_{i1}^*}{G^{i*}R^*}\left(\frac{1}{Q} - \texttt{LerchPhi}\left(\frac{1}{R^*}, 1, Q\right)\right)\right]. \tag{A.7}$$

After rearranging Eq. (A.7), $gr_i(s)$ is expressed as:

$$gr_i(s) = \frac{u_s^{i*}(r_2^*)}{(R^* - 1)} + \frac{\tau_{i1}^*}{G^{m*}R^*}\left[\frac{1}{Q} - \texttt{LerchPhi}\left(\frac{1}{R^*}, 1, Q\right)\right]. \tag{A.8}$$

Appendix B. Derivation of governing differential equation

Differentiating Eq. (15) twice with respect to s^*

$$\frac{\partial^4 \sigma_s^{f*}}{\partial s^{*4}} = -2\mathrm{A}_{1R}\left(\frac{1}{E^{i*}}\frac{\partial^2 \sigma_s^{i*}}{\partial s^{*2}} - \frac{\partial^2 \sigma_s^{f*}}{\partial s^{*2}}\right) - 2\mathrm{A}_{2R}r_2^*\left(\frac{1}{E^{m*}r_3^{*2}}\frac{\partial^2 \sigma_s^{f*}}{\partial s^{*2}} - \frac{1}{E^{m*}r_2^{*2}}\frac{\partial^2 \sigma_s^{f*}}{\partial s^{*2}}\right). \tag{B.1}$$

Equation (B.1) can be solved for σ_s^{f*} by expressing σ_s^{i*} in terms of σ_s^{f*}. To achieve the objective, consider the equilibrium equations along the r and s directions [46]:

$$\frac{\partial \sigma_r}{\partial r} + \frac{R}{R-r}\frac{\partial \tau_{rs}}{\partial s} + \frac{\sigma_s - \sigma_r}{R-r} = 0, \qquad \text{in r - direction} \tag{B.2a}$$

$$\frac{\partial \tau_{rs}}{\partial r} + \frac{R}{R-r}\frac{\partial \sigma_s}{\partial s} - \frac{2\tau_{rs}}{R-r} = 0. \qquad \text{in s - direction} \tag{B.2b}$$

As proposed in the shear-lag theory [24], we considered the shear stress of the form:

$$\tau_{rs} = \frac{f_0(s)r}{2} + \frac{f_1(s)}{r}. \tag{B.3}$$

Substituting Eq. (B.3) in Eq. (B.2)(b), along the s-direction of the fiber results in:

$$\frac{f_0(s)}{2} - \frac{f_1(s)}{r_1^{*2}} + \frac{R^*}{R^* - r_1^*}\frac{\partial \sigma_s^{f*}}{\partial s^*} - \frac{2}{R^* - r_1^*}\left(\frac{f_0(s)r_1^*}{2} + \frac{f_1(s)}{r_1^*}\right) = 0. \tag{B.4}$$

Solving Eq. (B.4) for $f_0(s)$:

$$\frac{f_0(s)}{2} = \frac{(R^*+1)}{(R^*-3)}f_1(s) - \frac{R^*}{(R^*-3)}\frac{\partial \sigma_s^{f*}}{\partial s^*}. \tag{B.5}$$

Similarly, applying the equilibrium equation along the s-direction for the interphase yields:

$$\frac{f_0(s)}{2} - \frac{f_1(s)}{r^{*2}} + \frac{R^*}{R^* - r^*}\frac{\partial \sigma_s^{i*}}{\partial s^*} - \frac{2}{R^* - r^*}\left(\frac{f_0(s)r_\beta^*}{2} + \frac{f_1(s)}{r^*}\right) = 0. \tag{B.6}$$

The interfacial shear stress between the interphase and matrix must be equal to the shear stress in the interphase at $r^* = r_2^*$. Therefore:

$$\frac{f_0(s)r^*}{2} + \frac{f_1(s)}{r^*} = \mathrm{A}_2\left[\frac{u_s^{m*}(r^*)}{(R^* - r^*)} - \frac{u_s^{m*}(r_2^*)}{(R^* - r_2^*)}\right]. \tag{B.7}$$

Solving Eq. (B.7) for $f_1(s)$:

$$f_1(s) = -\frac{f_0(s)r^{*2}}{2} + \mathrm{A}_2 r^*\left[\frac{u_s^{m*}(r^*)}{(R^* - r^*)} - \frac{u_s^{m*}(r_2^*)}{(R^* - r_2^*)}\right]. \tag{B.8}$$

Hence, $f_0(s)$ is estimated by substituting Eq. (B.8) into Eq. (B.5). The final expression of $f_0(s)$ after the mathematical simplifications:

$$f_0(s) = \frac{2(R^*+1)}{(R^*-3) + (R^*+1)r^{*2}}\mathrm{A}_2 r^*\left[\frac{u_s^{m*}(r^*)}{(R^* - r^*)} - \frac{u_s^{m*}(r_2^*)}{(R^* - r_2^*)}\right] - \frac{2R^*}{(R^*-3) + (R^*+1)r^{*2}}\frac{\partial \sigma_s^{f*}}{\partial s^*}. \tag{B.9}$$

Therefore, $f_1(s)$ is obtained by substituting Eq. (B.9) into Eq. (B.8):

$$f_1(s) = \left(\frac{(R^* - 3)}{(R^* - 3) + (R^* + 1)r^{*2}}\right) \mathrm{A}_2 r^* \left[\frac{u_s^{m*}(r^*)}{(R^* - r^*)} - \frac{u_s^{m*}(r_2^*)}{(R^* - r_2^*)}\right] + \frac{R^* r^{*2}}{(R^* - 3) + (R^* + 1)r^{*2})} \frac{\partial \sigma_s^{f*}}{\partial s^*} \tag{B.10}$$

Now both $f_0(s)$ and $f_1(s)$ are expressed in terms of σ_s^{f*} in Eqs. (B.9) and (B.10), respectively. Therefore, σ_s^{i*} can be obtained in terms of σ_s^{f*} substituting Eqs. (B.9) and (B.10) in Eq. (B.6):

$$\frac{\partial \sigma_s^{i*}(r^*)}{\partial s^*} = \mathrm{B}_2 \mathrm{A}_{2R} r^* \left[\frac{u_s^{m*}(r^*)}{(R^* - r^*)} - \frac{u_s^{m*}(r_2^*)}{(R^* - r_2^*)}\right] + \mathrm{B}_1 \frac{\partial \sigma_s^{f*}}{\partial s^*}, \tag{B.11}$$

where B_1 and B_2 are defined as:

$$\mathrm{B}_1 = \frac{2(R^* - r^*)}{(R^* - 3) + (R^* + 1)r^{*2}}, \tag{B.12a}$$

$$\mathrm{B}_2 = \left(\frac{(R^* + r^*)(R^* - 3)}{r^{*2}[(R^* - 3) + (R^* + 1)r^{*2}]} - \frac{(R^* - 3r^*)(R^* + 1)}{(R^* - 3) + (R^* + 1)r^{*2}}\right). \tag{B.12b}$$

After differentiating Eq. (B.11) with respect to 's^*' and using the constitutive laws, Eq. (B.11) becomes:

$$\frac{\partial^2 \sigma_s^{i*}(r^*)}{\partial s^{*2}} = \mathrm{B}_2 \mathrm{A}_{2R} r^* \left[\frac{1}{(R^* - r^*)} \frac{\sigma_s^{f*}}{E^{m*} r_3^{*2}} - \frac{1}{(R^* - r_2^*)} \frac{\sigma_s^{f*}}{E^{m*} r_2^{*2}}\right] + \mathrm{B}_1 \frac{\partial^2 \sigma_s^{f*}}{\partial s^{*2}}. \tag{B.13}$$

Substituting Eq. (B.13) into Eq. (B.1) leads to the below mentioned fourth order governing differential equation in σ_s^{f*}:

$$\begin{aligned} \frac{d^4 \sigma_s^{f*}}{ds^{*4}} = &- \left[\frac{2\mathrm{A}_{1R}(\mathrm{B}_1 - E^{i*})}{E^{i*}} + \left(\frac{2\mathrm{A}_{2R} r_2^*}{E^{m*} r_3^{*2}} - \frac{2\mathrm{A}_{2R} r_2^*}{E^{m*} r_2^{*2}}\right)\right] \frac{\mathrm{d}^2 \sigma_s^{f*}}{\mathrm{d}s^{*2}} \\ &- \frac{2\mathrm{A}_{1R}\mathrm{B}_2\mathrm{A}_{2R} r^*}{E^{i*}} \left[\frac{1}{(R^* - r^*)} \frac{1}{E^{m*} r_3^{*2}} - \frac{1}{(R^* - r_2^*)} \frac{1}{E^{m*} r_2^{*2}}\right] \sigma_s^{f*}. \end{aligned} \tag{B.14}$$

The partial derivative in Eq. (B.14) is treated as ordinary derivative, which can be expressed as Eq. (16).

Appendix C. Estimation of normal stresses in fiber

Normal stresses in the fiber are estimated by solving Eq. (16). Consider a solution of the form:

$$\sigma_s^{f*} = e^{\lambda s^*}, \tag{C.1}$$

Substituting Eq. (C.1) into the governing differential Eq. (16), a fourth order characteristic equation in λ is arrived. The four eigen values λ_1, λ_2, λ_3 and λ_4 of the characteristic equation are estimated as:

$$\lambda = \pm\sqrt{-K_1} \quad \text{and} \quad \pm\sqrt{K_2} \tag{C.2}$$

where,

$$\mathrm{K}_1 = \frac{\mathrm{T}_2 \pm \sqrt{\mathrm{T}_2^2 - 4\mathrm{T}_1}}{2}, \tag{C.3a}$$

$$\mathrm{K}_2 = \frac{-2\mathrm{T}_1}{\mathrm{T}_2 \pm \sqrt{\mathrm{T}_2^2 - 4\mathrm{T}_1}}. \tag{C.3b}$$

In this study, K_1 and K_2 are observed to be negative and positive, respectively. Hence, the eigen values are always positive. However, considering Eqs. (C.2) and (C.3), several combinations of eigen values are possible. The analytical results are observed to be in agreement with the results from finite element analysis for a particular set of eigen values: $\lambda_1 = -\sqrt{-K_{11}}, \lambda_2 = -\sqrt{-K_{12}}, \lambda_3 = \sqrt{K_{13}}$ and $\lambda_4 = \sqrt{K_{14}}$, where $K_{11} = \frac{\mathrm{T}_2 - \sqrt{\mathrm{T}_2^2 - 4\mathrm{T}_1}}{2}, K_{12} = \frac{\mathrm{T}_2 + \sqrt{\mathrm{T}_2^2 - 4\mathrm{T}_1}}{2}, K_{13} = \frac{-2\mathrm{T}_1}{\mathrm{T}_2 + \sqrt{\mathrm{T}_2^2 - 4\mathrm{T}_1}}$ and $K_{14} = \frac{-2\mathrm{T}_1}{\mathrm{T}_2 - \sqrt{\mathrm{T}_2^2 - 4\mathrm{T}_1}}$. Therefore, the total solution of the fiber normal stresses can be written as:

$$\sigma_s^{f*} = \mathrm{C}_1 e^{\lambda_1 s^*} + \mathrm{C}_2 e^{\lambda_2 s^*} + \mathrm{C}_3 e^{\lambda_3 s^*} + \mathrm{C}_4 e^{\lambda_4 s^*}. \tag{C.4}$$

Constants $\mathrm{C}_1, \mathrm{C}_2, \mathrm{C}_3$ and C_4 in Eq. (C.4) are estimated based on the below mentioned boundary conditions.

1. At s^*=0 (see Fig. 1), the fiber stress (σ_s^{f*}) is balanced by the stress at the fiber embedded end (σ_0^*). Therefore, $\sigma_s^{f*}(s^*=0)=\sigma_0^*$.

2. At s^*=L, the stress at the pulled end is balanced by the applied stress σ_{app}^*, estimated as the ratio of pull out force P_f to the fiber cross section area. Hence, $\sigma_s^{f*}(s^*=L^*)=\sigma_{app}^*$.

Considering perfect stress transfer, the shear forces on either ends of the fiber will be zero. Therefore, the first derivative of the fiber stress at either ends must be zero:

3. at s^*=0, $\frac{\partial\sigma_s^{f*}(s^*=0)}{\partial s^*}=0$ and

4. at s^*=L, $\frac{\partial\sigma_s^{f*}(s^*=L)}{\partial s^*}=0$.

Applying the above boundary conditions, the constants C_1, C_2, C_3 and C_4 are estimated as:

$$\mathrm{C}_1=\sigma_0^*-(\mathrm{C}_2+\mathrm{C}_3+\mathrm{C}_4), \tag{C.5a}$$

$$\mathrm{C}_2=\frac{\sigma_0^*\lambda_1-\mathrm{C}_3(\lambda_1-\lambda_3)-\mathrm{C}_4(\lambda_1-\lambda_4)}{(\lambda_1-\lambda_2)}, \tag{C.5b}$$

$$\mathrm{C}_3=\frac{(\sigma_0^*\lambda_2e^{\lambda_1L^*}-\sigma_{app}^*\lambda_2)-\mathrm{C}_4(\lambda_2-\lambda_4)(e^{\lambda_2L^*}-e^{\lambda_4L^*})}{(\lambda_2-\lambda_3)(e^{\lambda_2L^*}-e^{\lambda_3L^*})}, \tag{C.5c}$$

$$\mathrm{C}_4=\frac{(\sigma_0^*e^{\lambda_2L^*}-\sigma_{app}^*)\lambda_1(\lambda_2-\lambda_3)-(\sigma_0^*e^{\lambda_1L^*}-\sigma_{app}^*)\lambda_2(\lambda_1-\lambda_3)}{[\lambda_1\lambda_4+\lambda_2\lambda_3-\lambda_1\lambda_3-\lambda_2\lambda_4](e^{\lambda_2L^*}-e^{\lambda_4L^*})}. \tag{C.5d}$$

Appendix D. Pull-out force vs. fiber displacement

The relation between pull-out force and fiber displacement is established by considering the strain-displacement relation in the fiber along the 's' direction, as mentioned below:

$$\delta_f^*=\int_0^{L^*}\epsilon_s^{f*}ds^*=\int_0^{L^*}\sigma_s^{f*}ds^*, \tag{D.1}$$

Substituting the expression for σ_s^{f*} from Eq. (C.4) in Eq. (D.1):

$$\delta_f^*=\int_0^{L^*}\left[\mathrm{C}_1e^{\lambda_1s^*}+\mathrm{C}_2e^{\lambda_2s^*}+\mathrm{C}_3e^{\lambda_3s^*}+\mathrm{C}_4e^{\lambda_4s^*}\right]ds^*. \tag{D.2}$$

Therefore, the fiber displacement is estimated as a function of λ and fiber length L^* as:

$$\delta_f^*=\frac{\mathrm{C}_1}{\lambda_1}(e^{\lambda_1L^*}-1)+\frac{\mathrm{C}_2}{\lambda_2}(e^{\lambda_2L^*}-1)+\frac{\mathrm{C}_3}{\lambda_3}(e^{\lambda_3L^*}-1)+\frac{\mathrm{C}_4}{\lambda_4}(e^{\lambda_4L^*}-1). \tag{D.3}$$

Note that constants C_1-C_4 are functions of the applied stress on the fiber, which is in turn a function of the pull-out force. Therefore, the fiber displacements are estimated for the given pull-out force to generate a force-displacement curve.

Appendix E. Stresses in the interphase

Substituting the expression for σ_s^{f*} from Eqs. (C.4) in Eq. (18):

$$\frac{\partial^2\sigma_s^{i*}}{\partial s^{*2}}=(\mathrm{B}_3+\mathrm{B}_2\lambda_1^2)\mathrm{C}_1e^{\lambda_1s^*}+(\mathrm{B}_3+\mathrm{B}_2\lambda_2^2)\mathrm{C}_2e^{\lambda_2s^*}+(\mathrm{B}_3+\mathrm{B}_2\lambda_3^2)\mathrm{C}_3e^{\lambda_3s^*}+(\mathrm{B}_3+\mathrm{B}_2\lambda_4^2)\mathrm{C}_4e^{\lambda_4s^*}. \tag{E.1}$$

Hence, the stresses along the s-direction in the interphase can be obtained by integrating Eq. (E.1) twice:

$$\sigma_s^{i*}=\frac{(\mathrm{B}_3+\mathrm{B}_2\lambda_1^2)\mathrm{C}_1}{\lambda_1^2}e^{\lambda_1s^*}+\frac{(\mathrm{B}_3+\mathrm{B}_2\lambda_2^2)\mathrm{C}_2}{\lambda_2^2}e^{\lambda_2s^*}+\frac{(\mathrm{B}_3+\mathrm{B}_2\lambda_3^2)\mathrm{C}_3}{\lambda_3^2}e^{\lambda_3s^*}+\frac{(\mathrm{B}_3+\mathrm{B}_2\lambda_4^2)}{\lambda_4^2}\mathrm{C}_4e^{\lambda_4s^*}+\mathrm{H}_1s^*+\mathrm{H}_2. \tag{E.2}$$

The constants H_1 and H_2 are estimated considering the below mentioned boundary conditions for the interphase:

1. At s^*=0 (see Fig. 1), the interphase normal stress (σ_s^{i*}) is balanced by the specified stress at the fiber embedded end (σ_0^*). Therefore, $\sigma_s^{i*}(s^*=0)=\sigma_0^*$.

2. Considering a perfect stress transfer, the shear forces on either ends of the interphase will be zero. Therefore, the first derivative of the interphase normal stress at $s^* = 0$ must be zero, $\frac{\partial \sigma_s^{i*}(s^*=0)}{\partial s^*} = 0$.

Applying the above boundary conditions to Eq. (E.2), constants H_1 and H_2 are estimated as:

$$\mathrm{H}_1 = -\left[\frac{(\mathrm{B}_3 + \mathrm{B}_2\lambda_1^2)\mathrm{C}_1}{\lambda_1} + \frac{(\mathrm{B}_3 + \mathrm{B}_2\lambda_2^2)\mathrm{C}_2}{\lambda_2} + \frac{(\mathrm{B}_3 + \mathrm{B}_2\lambda_3^2)\mathrm{C}_3}{\lambda_3} + \frac{(\mathrm{B}_3 + \mathrm{B}_2\lambda_4^2)}{\lambda_4}\mathrm{C}_4\right], \tag{E.3a}$$

$$\mathrm{H}_2 = \sigma_0^* - \left[\frac{(\mathrm{B}_3 + \mathrm{B}_2\lambda_1^2)\mathrm{C}_1}{\lambda_1^2} + \frac{(\mathrm{B}_3 + \mathrm{B}_2\lambda_2^2)\mathrm{C}_2}{\lambda_2^2} + \frac{(\mathrm{B}_3 + \mathrm{B}_2\lambda_3^2)\mathrm{C}_3}{\lambda_3^2} + \frac{(\mathrm{B}_3 + \mathrm{B}_2\lambda_4^2)}{\lambda_4^2}\mathrm{C}_4\right]. \tag{E.3b}$$

Differentiating Eq. (8)(b) with respect to s^*:

$$\frac{\partial \tau_{i1}^*}{\partial s^*} = \mathrm{A}_2\left[\frac{1}{(R^* - r_2^*)}\frac{\partial u_s^{i*}(r_2^*)}{\partial s^*} - \frac{1}{(R^* - 1)}\frac{\partial u_s^{i*}(1)}{\partial s^*}\right] = \mathrm{A}_2\left[\frac{1}{(R^* - r_2^*)}\frac{\sigma_s^{f*}}{E^{m*}r_2^{*2}} - \frac{1}{(R^* - 1)}\sigma_s^{f*}\right]. \tag{E.4}$$

Using Eq. (C.4) in Eq. (E.4), yields:

$$\frac{\partial \tau_{i1}^*}{\partial s^*} = \mathrm{A}_3[\mathrm{C}_1 e^{\lambda_1 s^*} + \mathrm{C}_2 e^{\lambda_2 s^*} + \mathrm{C}_3 e^{\lambda_3 s^*} + \mathrm{C}_4 e^{\lambda_4 s^*}]. \tag{E.5}$$

where A_3 is given by:

$$\mathrm{A}_3 = \mathrm{A}_2\left[\frac{1}{E^{m*}r_2^{*2}(R^* - r_2^*)} - \frac{1}{(R^* - 1)}\right]. \tag{E.6}$$

Integrating Eq. (E.5)

$$\tau_{i1}^* = \mathrm{A}_3\left[\frac{\mathrm{C}_1}{\lambda_1}e^{\lambda_1 s^*} + \frac{\mathrm{C}_2}{\lambda_2}e^{\lambda_2 s^*} + \frac{\mathrm{C}_3}{\lambda_3}e^{\lambda_3 s^*} + \frac{\mathrm{C}_4}{\lambda_4}e^{\lambda_4 s^*}\right] + \mathrm{H}_3. \tag{E.7}$$

where H_3 is estimated based on the boundary condition, $\tau_{i1}^* = 0$ at $s^* = 0$:

$$\mathrm{H}_3 = -\mathrm{A}_3\left[\frac{\mathrm{C}_1}{\lambda_1} + \frac{\mathrm{C}_2}{\lambda_2} + \frac{\mathrm{C}_3}{\lambda_3} + \frac{\mathrm{C}_4}{\lambda_4}\right]. \tag{E.8}$$

Now, the interfacial stress between the interphase and matrix is estimated using Eq. (11):

$$\tau_{i2}^* = -\frac{1}{2r_2^*}\left[\mathrm{C}_1\left(\lambda_1 + \frac{2\mathrm{A}_3}{\lambda_1}\right)e^{\lambda_1 s^*} + \mathrm{C}_2\left(\lambda_2 + \frac{2\mathrm{A}_3}{\lambda_2}\right)e^{\lambda_2 s^*} + \mathrm{C}_3\left(\lambda_3 + \frac{2\mathrm{A}_3}{\lambda_3}\right)e^{\lambda_3 s^*} + \mathrm{C}_4\left(\lambda_4 + \frac{2\mathrm{A}_3}{\lambda_4}\right)e^{\lambda_4 s^*} + 2\mathrm{H}_3\right] \tag{E.9}$$

Therefore, shear stresses in the interphase and the matrix are estimated using Eq. (1).

Appendix F. Straight fiber pull-out test

Consider a straight fiber pull-out problem in a three phase system, as shown in Fig. F.1(a). In straight fiber pull out system, fiber, interphase and the matrix are co-axial. Therefore, the system is axi-symmetric. Let the modulus of elasticity and Poisson's ratio of the fiber, interphase and matrix are represented by E^f, E^i and E^m and ν^f, ν^i and ν^m, respectively. The radii of the fiber, coating and matrix are denoted by r_1, r_2 and r_3, respectively. Fiber is pulled by a force P_f. Tangential stresses in the r and x coordinate system in the interphase and matrix along with the interfacial shear stresses between fiber, interphase and interphase and matrix are indicated by τ_{rx}^i, τ_{rx}^m, τ_{i1} and τ_{i2}, respectively, refer to Fig. F.1(c). τ_{rx} is the shear stress at point r along the x direction. Equilibrium of stresses on a differential fiber element segment dx (see Fig. F.1(b)) yields:

$$(\sigma_x^{f*} + d\sigma_x^{f*})\pi r_1^{*2} - \sigma_x^{f*}\pi r_1^{*2} + \tau_{i1}^* 2\pi r_1^* dx^* + \tau_{i2}^* 2\pi r_2^* dx^* = 0. \tag{F.1}$$

Rearranging Eq. (F.1):

$$\frac{d\sigma_x^{f*}}{dx^*} = -2[\tau_{i1}^* + \tau_{i2}^* r_2^*]. \tag{F.2}$$

The strain-displacement relations in fiber, interphase and matrix can be written as:

$$\gamma_{rx}^{\varrho} = \frac{du_x^{\varrho*}}{dr^*} + \frac{du_r^{\varrho*}}{dx^*} \approx \frac{du_x^{\varrho*}}{dr^*} \tag{F.3}$$

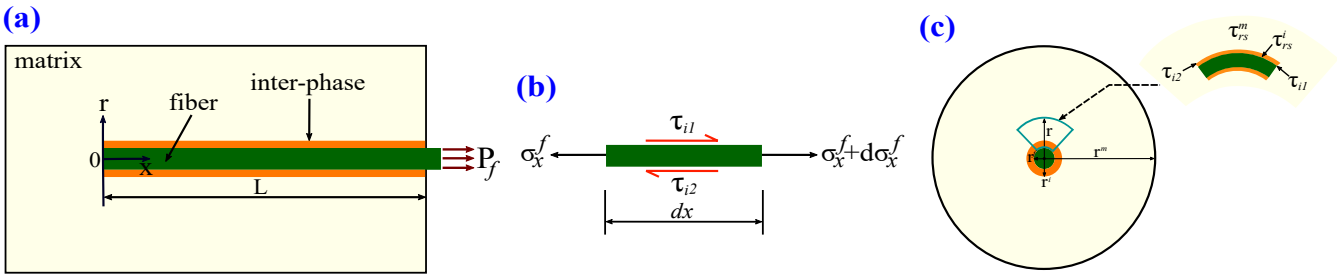

Figure F.1: (a) Schematic of a straight fiber surrounded by an interphase material, embedded in a polymer matrix. (b) Equilibrium of stresses in a differential fiber element segment dx. (c) Tangential stresses of a matrix segment of length dx along the radial direction. Shear stresses in the interphase and matrix along with the interfacial shear stresses between fiber-interphase and interphase-matrix are indicated by τ_{rx}^i, τ_{rx}^m, τ_{i1} and τ_{i2}, respectively.

where u indicates the displacement. Based on the matrix equilibrium:

$$\tau_{i2}^* = \tau_{rx}^{m*} r^*, \tag{F.4}$$

and hence,

$$\frac{du_x^{m*}}{dr^*} = \frac{\tau_{rx}^{m*}}{G^{m*}} = \frac{\tau_{i2}^*}{G^{m*} r^*}. \tag{F.5}$$

Therefore,

$$\int_{u_x^{m*}(r_2^*)}^{u_x^{m*}(r^*)} du_x^{m*} = \int_{r_2^*}^{r^*} \frac{\tau_{i2}^*}{G^{m*}} \frac{dr^*}{r^*}, \tag{F.6a}$$

$$u_x^{m*}(r^*) - u_x^{m*}(r_2^*) = \frac{\tau_{i2}^*}{G^{m*}} \ln(r^*). \tag{F.6b}$$

By rearranging Eq. (F.6)(b):

$$\tau_{i2}^* = \frac{G^{m*}}{\ln(r^*)} [u_x^{m*}(r^*) - u_x^{m*}(r_2^*)]. \tag{F.7}$$

In the similar lines:

$$\tau_{i1}^* = \frac{G^{i*}}{\ln(r^*)} [u_x^{i*}(r^*) - u_x^{f*}]. \tag{F.8}$$

Substituting Eq. (F.8) and (F.7) into Eq. (F.2) yields:

$$\frac{d\sigma_x^{f*}}{dx^*} = -2 \left(\frac{G^{i*}}{\ln(r^*)} [u_x^{i*}(r^*) - u_x^{f*}] + \frac{G^{m*} r_2^*}{\ln(r^*)} [u_x^{m*}(r^*) - u_x^{m*}(r_2^*)] \right). \tag{F.9}$$

In the similar lines of curved fiber analysis, after mathematical simplification using the stress-strain relations and differentiation, Eq. (F.9) can be written as:

$$\frac{d^2\sigma_x^{f*}}{dx^{*2}} = -2 \left(\frac{G^{i*}}{\ln(r^*)} \left[\frac{\sigma_x^{i*}}{E^{i*}} - \sigma_x^{f*} \right] + \frac{G^{m*} r_2^*}{\ln(r^*)} \left[\frac{\sigma_x^{f*}}{E^{m*} r^{*2}} - \frac{\sigma_x^{f*}}{E^{m*} r_2^{*2}} \right] \right). \tag{F.10}$$

Therefore, the governing differential equation can be derived by differentiating Eq. (F.10) twice with respect to x^* as given below:

$$\frac{d^4\sigma_x^{f*}}{dx^{*4}} + R_1 \frac{d^2\sigma_x^{i*}}{dx^{*2}} + R_2 \frac{d^2\sigma_x^{f*}}{dx^{*2}} = 0 \tag{F.11}$$

where,

$$R_1 = -\frac{2G^{i*}}{E^{i*} \ln(r^*)}, \tag{F.12a}$$

$$R_2 = \frac{2G^{i*}}{\ln(r^*)} - \frac{2G^{m*} r_2^*}{\ln(r^*)} \left[\frac{1}{E^{m*} r^{*2}} - \frac{1}{E^{m*} r_2^{*2}} \right]. \tag{F.12b}$$

Applying the equilibrium equations (B.2) for straight fiber after neglecting the radial stresses:

$$\frac{\partial \tau_{rx}}{\partial x} = 0, \qquad \text{along the r - direction} \tag{F.13a}$$

$$\frac{\partial \tau_{rx}}{\partial r} + \frac{\partial \sigma_x}{\partial x} = 0. \qquad \text{along the x - direction} \tag{F.13b}$$

Based on the shear-lag theory, consider the shear stress of the form [24]:

$$\tau_{rx} = \frac{f_0(x) r}{2} + \frac{f_1(x)}{r}. \tag{F.14}$$

Hence, after the mathematical simplifications, the governing equation in terms of the axial stresses can be written as:

$$\frac{d^2 \sigma_x^{i*}}{dx^{*2}} = \frac{2r_2^*}{r^{*2} - r_2^{*2}} \frac{G^{m*}}{\ln(r^*)} \left(\frac{1}{E^{m*} r^{*2}} - \frac{1}{E^{m*} r_2^{*2}} \right) \sigma_x^{f*} = J_1 \sigma_x^{f*}, \tag{F.15}$$

where,

$$J_1 = \frac{2r_2^*}{r^{*2} - r_2^{*2}} \frac{G^{m*}}{\ln(r^*)} \left(\frac{1}{E^{m*} r^{*2}} - \frac{1}{E^{m*} r_2^{*2}} \right). \tag{F.16}$$

Therefore, the governing differential Eq. (F.11) can be written as

$$\frac{d^4 \sigma_x^{f*}}{dx^{*4}} + S_1 \frac{d^2 \sigma_x^{f*}}{dx^{*2}} + S_2 \sigma_x^{f*} = 0. \tag{F.17}$$

where, $S_1 = R_2$ and $S_2 = J_1 R_1$. The solution of Eq. (F.17) can be expressed as:

$$\sigma_x^{f*} = \mathrm{D}_1 e^{\lambda_1 x^*} + \mathrm{D}_2 e^{\lambda_2 x^*} + \mathrm{D}_3 e^{\lambda_3 x^*} + \mathrm{D}_4 e^{\lambda_4 x^*}. \tag{F.18}$$

Therefore, Eq. (F.18) can be solved considering the boundary conditions as in the case of curved fiber, refer to Appendix B and Appendix C.

Similarly, the interfacial stresses (τ_{i1}^*, τ_{i2}^*) can be estimated considering Eqs. (F.8) and(**??**), respectively. The first derivative of Eq. (F.8) is given by:

$$\frac{d\tau_{i1}^*}{dx^*} = \frac{G^{i*}}{\ln(r^*)} \left(\frac{1}{E_m^* r_2^{*2}} - 1 \right) \sigma_f^* = S_3 \sigma_f^* \tag{F.19}$$

where $S_3 = \frac{G^{i*}}{\ln(r^*)} \left(\frac{1}{E_m^* r_2^{*2}} - 1 \right)$. Substituting Eq. (F.18) in Eq. (F.19) and integrating:

$$\tau_{i1}^* = S_3 \left[\frac{\mathrm{D}_1}{\lambda_1} e^{\lambda_1 x^*} + \frac{\mathrm{D}_2}{\lambda_2} e^{\lambda_2 x^*} + \frac{\mathrm{D}_3}{\lambda_3} e^{\lambda_3 x^*} + \frac{\mathrm{D}_4}{\lambda_4} e^{\lambda_4 x^*} \right] + R_3, \tag{F.20}$$

where R_3 can be obtained considering the boundary condition that at $x^* = 0, \tau_{i1}^* = 0$:

$$R_3 = -S_3 \left[\frac{\mathrm{D}_1}{\lambda_1} + \frac{\mathrm{D}_2}{\lambda_2} + \frac{\mathrm{D}_3}{\lambda_3} + \frac{\mathrm{D}_4}{\lambda_4} \right]. \tag{F.21}$$

Therefore, τ_{i2} can be estimated from Eq. (F.2):

$$\tau_{i2}^* = -\frac{1}{2r_2^*} \left[\mathrm{D}_1 \lambda_1 e^{\lambda_1 s^*} + \mathrm{D}_2 \lambda_2 e^{\lambda_2 s^*} + \mathrm{D}_3 \lambda_3 e^{\lambda_3 s^*} + \mathrm{D}_4 \lambda_4 e^{\lambda_4 s^*} + 2\tau_{i1}^* \right]. \tag{F.22}$$

Finally, the shear stresses in the interphase and the matrix are estimated from constitutive relations in Eq. (1).